JOURNAL OF AIRCRAFT
Vol. 47, No. 4, July–August 2010

Prediction of Nonlinear Rolling and Magnus Coefficients of Cruciform-Finned Missiles

J. Morote* and G. Liaño†
National Institute of Aerospace Technology, 28850 Madrid, Spain

DOI: 10.2514/1.47212

A new method based on strip and slender-body theories has been developed to predict the aerodynamic roll and wing-induced Magnus coefficients of cruciform-tailed missiles at high angles of attack. The method is applicable over the Mach number range, up to large angles of attack at arbitrary bank angles, providing analytical expressions of the nonlinear rolling moments: roll damping, roll driving, induced roll moments, and additional coupling terms. The analytical expressions fit the form of the Maple–Synge expansion and the degree of nonlinearity shown by experimental results.

Nomenclature

C_F	=	$F/(qS_w)$, force coefficient
Cl	=	$L/(qS_wD)$, roll-moment coefficient
C_N	=	$N/(qS_w)$, normal-force coefficient
$C_{N\alpha w}$	=	angle-of-attack coefficient of the wing-alone normal force
C_Y	=	$F_Y/(qS_w)$, side-force coefficient
D	=	reference length, missile diameter
F_y	=	force along Y axis, side force
F_z	=	force along Z axis
L	=	roll moment
N	=	$-F_z$, normal force
p	=	roll rate
q	=	dynamic pressure
S_w	=	wing area (two panels)
V	=	speed of missile
V_n	=	component of speed normal to missile axis
δ_T	=	fin cant deflection
φ	=	bank angle

Subscripts

sbt	=	slender-body theory
wb	=	wing in presence of body

I. Introduction

THE performance of unguided cruciform-tailed missiles critically depends on the ability to reduce dispersion due to slight configurational asymmetries by spinning at a low-amplitude motion. Design spin rates are kept low in order to avoid Magnus instability, sometimes favoring the occurrence of roll–yaw coupling by the action of induced roll moments. The missile fails to reach its design rolling velocity that remains locked to the pitch frequency [1], occasionally resulting in high-amplitude motions. The prediction of the rolling motion at high angles of attack is critical to understand the flight performance of unguided cruciform configurations. This paper presents a new application of the strip and slender-body theories that provides analytical expressions of the nonlinear rolling moments: roll-damping moment, roll-driving moment, induced roll moment, and coupling terms. Additionally, fin contribution to Magnus characteristics can be obtained. The method is based on the wing-alone lifting capabilities obtained from experimental databases or aerodynamic codes at the Mach number of interest. The fin span loading of the slender-body theory [2] (SBT) provides the interference functions that determine the effective angle-of-attack distribution along the wing span. In this way, the effective angle of attack seen by the fin strips, and the wing-alone lifting capabilities are used to calculate the rolling derivatives induced by the wing-normal forces in the presence of the body. The nonlinear rolling derivatives are expressed as power series of the effective angle of attack seen by the strips. In addition to this central hypothesis and the assumptions underlying the strip and the SBT, the present method is a steady-state nonviscous method (with the exception of the wing-alone viscous effects). The roll damping and the Magnus side force due to the body are assumed to be negligible, and the loads on the panels are calculated in the absence of body vortex shedding. Comparison of the method to a reduced set of experimental results shows reasonable agreement up to moderate angles of attack, although additional wing-alone, and the corresponding wing-body, data are required for further validation.

Presented as Paper 2009-5716 at the AIAA Atmospheric Flight Mechanics Conference, Chicago, IL, 10–13 August 2009; received 16 September 2009; revision received 26 March 2010; accepted for publication 19 May 2010.

*Research Engineer, Aerodynamics Branch, INTA, Torrejón de Ardoz. Senior Member AIAA.

†Research Engineer, Aerodynamics Branch, INTA, Torrejón de Ardoz. Senior Member AIAA.

II. Description of the Method

In this work, the angle of attack is defined by $\delta = \sin\alpha = V_n/V$, where V is the velocity of the missile, V_n is the component of V normal to the missile axis, and α is the angle between this axis and the velocity direction. Given a cruciform configuration in the + position (panel geometry depicted in Fig. 1), the wing-alone normal-force coefficient in the absence of the body, calculated by strip theory, is

$$C_{Nw} = \frac{2}{S_w}\int_a^b C_{N\alpha w0}\delta c(y)\,\mathrm{d}y \tag{1}$$

The coefficient $C_{N\alpha w0}$ is the slope of the panel-normal-force curve at an angle of attack in the linear range. The factor 2 takes account of the opposite horizontal panel. Equation (1) does not include tip effects. If the wing is placed on a body of revolution of diameter D, the wing-normal-force coefficient in the presence of the body is now

$$C_{NwB} = \frac{2}{S_w}\int_a^b C_{N\alpha w0}\delta(y)c(y)\,\mathrm{d}y = \frac{2}{S_w}\int_a^b C_{N\alpha w0}\delta h(y)c(y)\,\mathrm{d}y \tag{2}$$

in which the effective angle of attack seen by the strips $\delta(y) = \delta h(y)$ varies spanwise due to the upwash field of the body. Equation (2) can be rewritten as

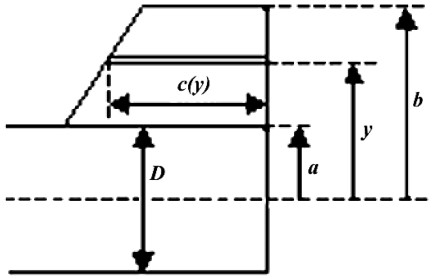

Fig. 1 Panel geometry.

$$C_{NwB} = \frac{2}{S_w}\int_a^b C_{N\alpha w0}\delta F(y)\,\mathrm{d}y$$

where $F(y) = h(y)c(y)$ can be considered the modified (due to the presence of the body) normal-force-generating capability of the strip situated at station y at the unperturbed angle of attack δ. $F(y)$ can be made nondimensional $f(y) = \frac{F(y)}{D}$, giving

$$C_{NwB} = \frac{2}{S_w}\int_a^b C_{N\alpha w0}\delta f(y) D\,\mathrm{d}y \tag{3}$$

By comparison with Eq. (2), $\delta f(y)$ is the effective angle of attack seen by the strips of a rectangular wing of constant chord D that generates, station by station, the same normal force as the original wing. The normal force developed by the wing in the presence of the body of Eq. (3) is independent of the exact shape of the wing panels. To obtain a form of $f(y)$, the SBT [2] can be used, and Eq. (3) then takes the form

$$\begin{aligned} C_{NwB\mathrm{sbt}} &= \frac{2}{S_w}\int_a^b C_{N\alpha w0\mathrm{sbt}}\,\delta f(y)_{\mathrm{sbt}} D\,\mathrm{d}y \\ &= \frac{2}{S_w}\int_a^b 4\delta\left[\left(b+\frac{a^2}{b}\right)^2 - \left(y+\frac{a^2}{y}\right)^2\right]^{1/2}\mathrm{d}y \end{aligned} \tag{4}$$

where $C_{N\alpha w0\mathrm{sbt}} = 2\pi(b-a)^2/S_w$. The integrand is the SBT span loading, which is independent of the exact shape of the wing panels. From this expression, we obtain

$$f(y)_{\mathrm{sbt}} = \frac{4}{C_{N\alpha w0\mathrm{sbt}} D}\left[\left(b+\frac{a^2}{b}\right)^2 - \left(y+\frac{a^2}{y}\right)^2\right]^{1/2} \tag{5}$$

By assuming $f(y) = f(y)_{\mathrm{sbt}}$, Eq. (3) gives

$$C_{NwB} = K_w C_{N\alpha w0}\delta \tag{6}$$

where

$$K_w = \frac{4}{\pi(b-a)^2}\int_a^b\left[\left(b+\frac{a^2}{b}\right)^2 - \left(y+\frac{a^2}{y}\right)^2\right]^{1/2}\mathrm{d}y \tag{7}$$

K_w is the wing interference factor of the SBT. Unlike Eq. (1), Eq. (3) includes tip effects if the interference function is taken as $f(y) = f(y)_{\mathrm{sbt}}$.

A reasonable extension of Eqs. (3) or (6) into the nonlinear range of angles of attack is

$$\begin{aligned} C_{NwB} &= \frac{2}{S_w}\int_a^b (C_{N\alpha w0}\delta + C_{N\alpha w2}\delta^3 + C_{N\alpha w4}\delta^5 + \cdots) f(y) D\,\mathrm{d}y \\ &= K_w C_{Nw} \end{aligned} \tag{8}$$

The linear behavior of Eq. (6), accurate enough at low angles of attack, is replaced in Eq. (8) by the experimental or calculated wing-alone normal-force coefficient C_{Nw} at the angle of attack δ. Equation (8) implicitly assumes that the interference function $f(y)$ and K_w are unaffected by the angle of attack, requiring empirical corrections in other methods [3]. The approach taken in the present work is based on the assumption that the expansion of Eq. (8) should be made in terms of the effective angle of attack $\delta f(y)$ seen by the strips. According to this assumption,

$$\begin{aligned} C_{NwB} = \frac{2}{S_w}\int_a^b \{&C_{N\alpha w0}[\delta f(y)] + C_{N\alpha w2}[\delta f(y)]^3 \\ &+ C_{N\alpha w4}[\delta f(y)]^5 + \cdots\} D\,\mathrm{d}y \end{aligned} \tag{9}$$

Since the horizontal panel-normal force is an odd function of the angle of attack, only odd powers of the effective angle of attack are used, making Eq. (9) applicable to negative angles of attack. It is implicitly assumed that the wing panels have no camber, so the normal force at a negative angle of attack is the negative of that at the same positive angle.

If the configuration is now banked in the positive direction an angle φ, as depicted in Fig. 2, the unperturbed angle of attack seen by the strips on panel 2 is $\delta\cos\varphi$, and the normal-force coefficient generated at low angles of attack by panel 2, projected in the crossflow direction indicated by δ, is

$$C_{NwB\langle 2\rangle} = \frac{\cos\varphi}{S_w}\int_a^b C_{N\alpha w0}\delta\cos\varphi[f(y) + g(y)\delta\sin\varphi] D\,\mathrm{d}y \tag{10}$$

where the effective angle of attack seen by the strips on panel 2 is $\delta\cos\varphi[f(y) + g(y)\delta\sin\varphi]$. The pattern of interference in Eq. (10) was taken from the SBT [2].

As before, Eq. (10) can be particularized for the SBT, and $g(y)$ can be approximated by $g(y)_{\mathrm{sbt}}$, where

$$g(y)_{\mathrm{sbt}} = \frac{4\sqrt{2}[y^4 - a^4]^{3/2}}{ARy^5 C_{N\alpha w0\mathrm{sbt}} D}[F(\psi_1, k) + F(\psi_2, k')] \tag{11}$$

F is the elliptic integral of the first kind, and

$$\cos\psi_1 = \frac{b(y^2-a^2)}{y(b^2-a^2)}; \qquad \cos\psi_2 = \frac{b(y^2+a^2)}{y(b^2+a^2)}$$

$$k^2 = \frac{(y^2+a^2)^2}{2(y^4+a^4)}; \qquad k'^2 = \frac{(y^2-a^2)^2}{2(y^4+a^4)}$$

The extension of Eq. (10) into the nonlinear range is, according to the previous assumption,

$$\begin{aligned} C_{NwB\langle 2\rangle} = \frac{\cos\varphi}{S_w}\int_a^b \{&C_{N\alpha w0}\delta\cos\varphi[f(y) + g(y)\delta\sin\varphi] \\ &+ C_{N\alpha w2}\delta^3\cos^3\varphi[f(y) + g(y)\delta\sin\varphi]^3 \\ &+ C_{N\alpha w4}\delta^5\cos^5\varphi[f(y) + g(y)\delta\sin\varphi]^5 + \cdots\} D\,\mathrm{d}y \end{aligned} \tag{12}$$

Equation (12) can be rewritten as

$$\begin{aligned} C_{NwB\langle 2\rangle} = \cos\varphi\int_a^b \{&C_{N\alpha 0}\delta\cos\varphi[f + g\delta\sin\varphi] \\ &+ C_{N\alpha 2}\delta^3\cos^3\varphi[f + g\delta\sin\varphi]^3 \\ &+ C_{N\alpha 4}\delta^5\cos^5\varphi[f + g\delta\sin\varphi]^5 + \cdots\}\,\mathrm{d}r \end{aligned} \tag{13}$$

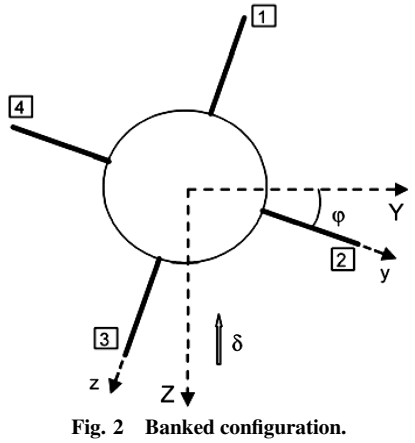

Fig. 2 Banked configuration.

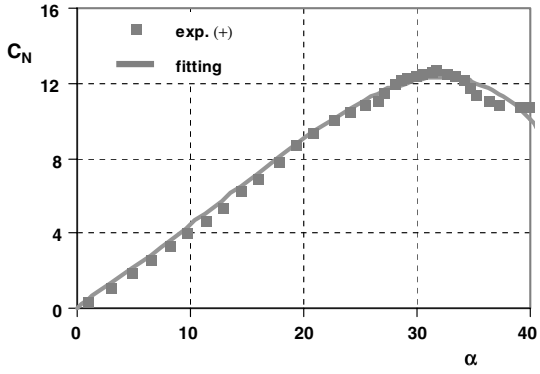

Fig. 3 Wing on body-normal force at + position (Mach 0.1).

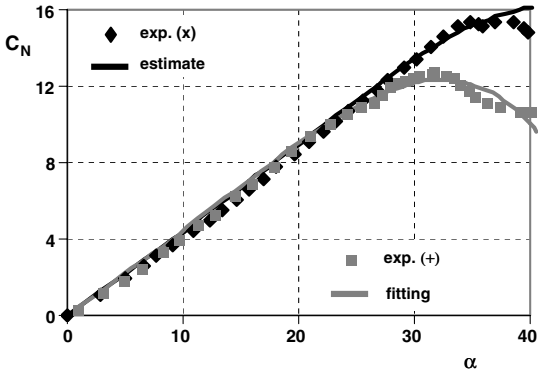

Fig. 4 Wing on body-normal force at + and × positions (Mach 0.1).

where the subscript w, indicating wing-alone coefficients, was removed, $f(y)$ and $g(y)$ were replaced by f and g, respectively, and $\mathrm{d}r = (D/S_W)\mathrm{d}y$ in order to abbreviate the expression.

III. Wing-Normal Force in the Presence of the Body

The calculation of the normal-force coefficient generated by the four panels is developed in Appendix A up to seventh order. The result given by Eq. (A2) is

$$\begin{aligned} C_{NwB} = 2\delta\{&C_{N\alpha 0}W^{100} + \tfrac{3}{4}C_{N\alpha 2}W^{300}\delta^2 \\ &+ \tfrac{1}{8}(3C_{N\alpha 2}W^{120} + 5C_{N\alpha 4}W^{500})\delta^4 \\ &+ \tfrac{1}{64}(50C_{N\alpha 4}W^{320} + 35C_{N\alpha 6}W^{700})\delta^6 \\ &+ \cos 4\varphi[\tfrac{1}{4}C_{N\alpha 2}W^{300}\delta^2 - \tfrac{3}{8}(3C_{N\alpha 2}W^{120} - C_{N\alpha 4}W^{500})\delta^4 \\ &- \tfrac{1}{16}(10C_{N\alpha 4}W^{320} - 7C_{N\alpha 6}W^{700})\delta^6] \\ &+ \cos 8\varphi[-\tfrac{1}{64}(10C_{N\alpha 4}W^{320} - C_{N\alpha 6}W^{700})\delta^6]\} \end{aligned} \tag{14}$$

The expression of Eq. (14) fits the in-plane Maple–Synge [4] expansion for the normal force [Eq. (B6) of Appendix B]. The out-of-plane component is presented in Eq. (A3). Equation (14) gives the analytical form of the terms as functions of the wing-alone coefficients and the weighting factors W^{nml} introduced in Eq. (A1) of Appendix A. The weighting factors give the influence of each of the wing-alone coefficients on the global coefficient. They depend only on the a/b ratio and the wing AR, and their evaluation is performed numerically. The values of the weighting factors appearing in this work are listed in Appendix C for ready use. Equation (14) is theoretically applicable up to large angles of attack at any Mach number, because the Mach number dependency enters through the wing-alone normal-force coefficients. For the cruciform configuration in the + attitude, Eq. (14) simply gives

$$\begin{aligned} C_{NwB\langle+\rangle} = 2\delta(&C_{N\alpha 0}W^{100} + C_{N\alpha 2}W^{300}\delta^2 \\ &+ C_{N\alpha 4}W^{500}\delta^4 + C_{N\alpha 6}W^{700}\delta^6) \end{aligned} \tag{15}$$

where $2W^{100} = K_W$ is the SBT wing-body interference factor. In the × attitude, Eq. (14) gives

$$\begin{aligned} C_{NwB\langle\times\rangle} = 2\delta[&C_{N\alpha 0}W^{100} + \tfrac{1}{2}C_{N\alpha 2}W^{300}\delta^2 \\ &+ (\tfrac{1}{4}C_{N\alpha 4}W^{500} + \tfrac{3}{2}C_{N\alpha 2}W^{120})\delta^4 + (\tfrac{1}{8}C_{N\alpha 6}W^{700} + \tfrac{5}{4}C_{N\alpha 4}W^{320})\delta^6] \end{aligned} \tag{16}$$

Reference [5] offers experimental wing on body-normal-force coefficients of a cruciform configuration ($a/b = 0.25$ and $AR = 1.5$) in the + and × attitudes, at Mach number 0.1, that can be compared with the predictions provided by the present method. Figure 3 depicts the experimental wing on the body-normal-force coefficient in the + position, together with the least-squares fitting of the experimental values, up to an angle of attack above the wing vortex breakdown.

The coefficients of the least-squares polynomial are the products of Eq. (15) for the + attitude: $2C_{N\alpha 0}W^{100}$, $2C_{N\alpha 2}W^{300}$, $2C_{N\alpha 4}W^{500}$, and $2C_{N\alpha 6}W^{700}$. Upon calculation of the weighting factors (Appendix C), an estimate of the wing-alone coefficients is obtained. From the wing-alone coefficients and the weighting factors of Eq. (16), the wing on the body-normal-force coefficient at the × attitude can be obtained. Figure 4 depicts the experimental result corresponding to the × position and the estimate provided by Eq. (16), together with the curves of Fig. 3.

Figure 5 presents the comparison between experimental results and the estimates of Eq. (16) for the configuration of [3] (pp. 237–239) with an $a/b = 0.5$ and $AR = 0.5$. It is apparent from the figure that the method overestimates the roll-orientation dependency of this configuration at Mach = 2.

If an assumption regarding the body carryover load is made, for example,

$$C_{NwB}/C_{NBw} = C_{NwB}/C_{NBw}|_{\text{linear}}$$

and an estimate of the body-alone normal force at the angle of attack is available, the present method might be an alternative to calculate

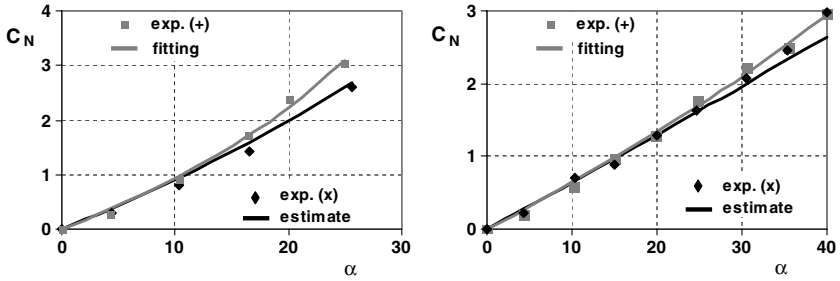

a) Mach 0.6 **b) Mach 2.0**

Fig. 5 Wing on body-normal force at + and × positions.

the normal force of cruciform configurations. However, the true aim of this work is the nonlinear roll derivatives of cruciform configurations, for which only the wing-normal-force components in the presence of the body are relevant. In addition, the theoretical methods to predict the roll derivatives are very limited (see the exhaustive survey made by Moore and Moore [6] concerning the roll-damping coefficient). Also, Magnus force will be addressed in Sec. V.

IV. Nonlinear Rolling Moments

The roll moment given by the span load distribution is derived in Appendix D. Equations (D1–D10) give the components corresponding to an independent term and terms in δ_T, p, $\delta_T p$, δ_T^2, p^2, $\delta_T p^2$, $\delta_T^2 p$, δ_T^3, and p^3 that fit the corresponding Maple–Synge [4] expansion [Eqs. (B11) and (B12) of Appendix B]. The independent term is the induced roll moment, the term in δ_T is the linear roll-driving moment, the term in p is the linear roll-damping moment, and the term in p^3 is the cubic roll-damping moment.

To assess the performance of the nonlinear rolling derivatives estimates developed in Appendix D, the method will be compared with the empirical correlation of Eastman [7] for cruciform configurations and subsequently extended by Mikhail [8] to wraparound, offset, and arbitrary number of fins. This correlation gives the ratio between the linear roll damping and the roll-driving coefficients at all regimes:

$$C_{lp}/C_{l\delta_T} = -2.15(y_c/D)$$

where $C_{lp} = \partial C_l/\partial(pD/2V)$, and y_c is the distance between the body axis and the area center of one panel. According to the present method, at low angles of attack (Appendix D),

$$C_{lp}/C_{l\delta_T} = -2(4C_{N\alpha 0}W^{102}/4C_{N\alpha 0}W^{101}) = -2(W^{102}/W^{101})$$

where the factor 2 was included to make this ratio comparable to the Eastman's ratio [7], because the definition of linear damping in this work is $C_{lp} = \partial C_l/\partial(pD/V)$. The two involved weighting factors only depend on the a/b ratio (Appendix C). Both expressions can be applied to the cruciform configurations, depicted in Fig. 6. The correlation of Eastman gives ($\lambda = a/b$) 1) the rectangular wing,

$$C_{lp}/C_{l\delta_T} = -2.15\frac{y_c}{D} = -2.15\frac{(1+\lambda)}{4\lambda}$$

and 2) the triangular wing,

$$C_{lp}/C_{l\delta_T} = -2.15\frac{y_c}{D} = -2.15\frac{(1+2\lambda)}{6\lambda}$$

Figure 7 presents the Eastman's correlation results [7] for rectangular and triangular wings vs λ, together with the estimate given by the present method that is independent of the planform shape of the wing.

In addition to the former linear application, the present method can be used to investigate the nonlinear behavior of the induced roll moment for cruciform configurations at low velocities [9,10].

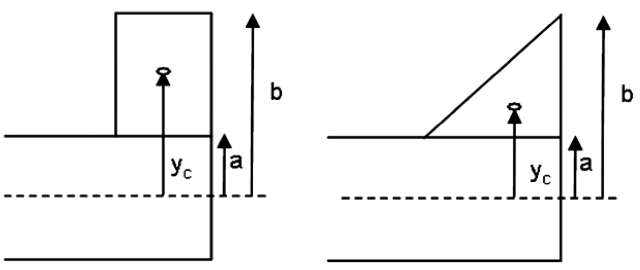

Fig. 6 Cruciform configurations.

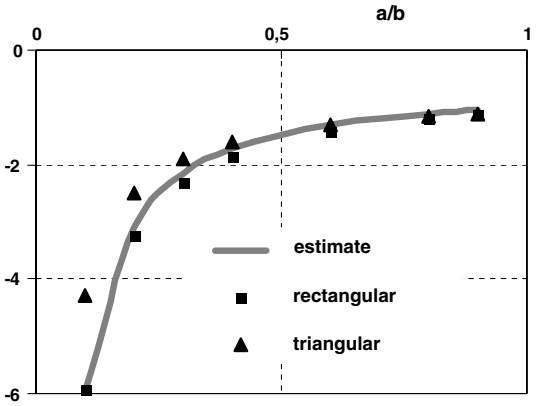

Fig. 7 Roll-damping-to-roll-driving ratio.

As schematically depicted in Fig. 8, at roll position $\varphi = 22.5°$ and low angles of attack, the roll moment is negative, changing sign at an angle of attack of $\alpha^* \sim 13$–$15°$. According to the present method, the induced roll moment at $\varphi = 22.5°$ (Appendix D), up to moderate angles of attack, can be represented by the following sixth-order polynomial:

$$C_l(\text{ind.}) = (-\tfrac{3}{2}C_{N\alpha 2}W^{211} - \tfrac{5}{2}C_{N\alpha 4}W^{411}\delta^2)\delta^4 \qquad (17)$$

The estimate provided by this expression can be compared with the experimental results for the basic finner given in [11]. This rocket has rectangular fins with $a/b = 0.33$ and $AR = 2$. Figure 9a presents the experimental [12] normal-force coefficient of a rectangular wing of $AR = 2$ at low velocities, together with the least-squares fitting, to obtain the wing-alone coefficients. Figure 9b presents the experimental [11] results of the induced roll moment together with the estimate provided by the method. The angle of attack at which the estimate changes sign is 10°. The present method predicts a similar behavior at any Mach number, as long as $C_{N\alpha 2}$ is positive and $C_{N\alpha 4}$ negative ($AR \leq 2$).

Figure 10b presents the comparison between the roll-damping coefficient estimates and the experimental values given in [6] for the basic finner at two supersonic Mach numbers. The AP05 code [13] was used to set the value of $C_{N\alpha 0}$. The coefficient $C_{N\alpha 2}$ was obtained by fitting the wing-alone data provided by code, as shown in Fig. 10a. The cubic component given by Eq. (D4) was disregarded, since $(-\frac{pD}{V})^3$ is negligible at supersonic speeds.

Finally, the method will be applied to the experimental results given in [14], obtained again for the basic finner at low speeds. According to the experiment, the steady-state spin of the rocket, with and without fin cant, as the angle of attack increases is schematically depicted in Fig. 11.

For the case of no-fin cant, the steady-state spin is zero, up to an angle of attack where breakout occurs. From this point, the rocket spins at an increasing rate in the positive or negative directions. The dual spin rates are nearly equal at a given angle of attack. If the fins are canted in the positive direction, the breakout also occurs in the positive direction. At higher angles of attack, the breakout can take place in either direction. According to the present model, when the

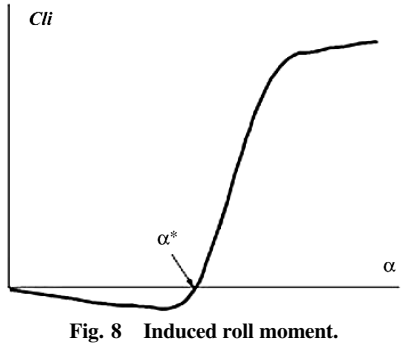

Fig. 8 Induced roll moment.

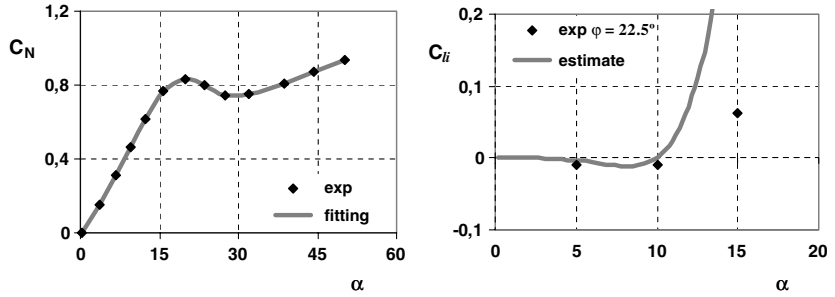

a) Normal-force fitting of experiment

b) Induced roll-moment estimate vs. experiment

Fig. 9 Basic finner wing-alone normal-force and induced roll-moment coefficients.

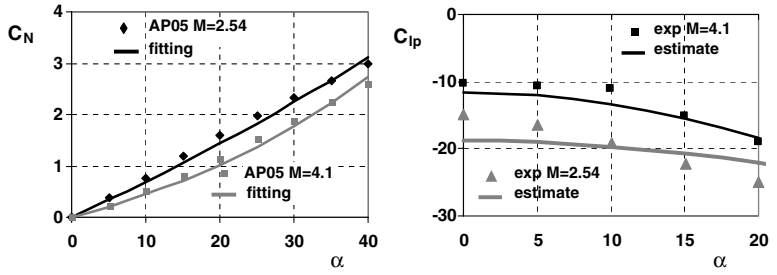

a) Normal-force fittings

b) Roll-damping estimates vs. experiment

Fig. 10 Basic finner normal-force and roll-damping moment coefficients.

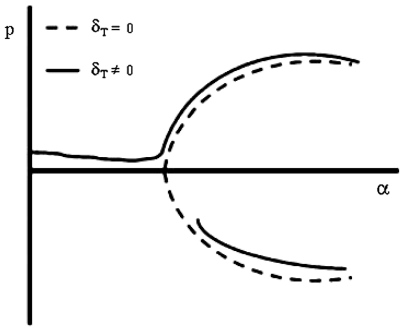

Fig. 11 Steady-state spin vs angle of attack.

fin cant is zero, the steady-state spin ($C_l = 0$) is the result of the equilibrium between the induced roll component of Eq. (D3), the linear damping component of Eq. (D2), and the cubic damping component of Eq. (D4):

$$C_l = C_l(\text{ind.}) + C_l(p) + C_l(p^3) = 0 \tag{18}$$

Possible solutions of Eq. (18) occur when

$$p = 0 \rightarrow C_l(\text{ind.}) = [\sin 4\varphi h_1(\delta) + \sin 8\varphi h_2(\delta)]$$
$$= \sin 4\varphi[h_1(\delta) + 2\cos 4\varphi h_2(\delta)] = 0 \tag{19}$$

Equation (19) yields the following:

1) $\sin 4\varphi = 0 \quad \forall\ \delta$ implies that the equilibrium for $p = 0$ occurs in the + or the × position

2) $\cos 4\varphi = [h_1(\delta)]/[2h_2(\delta)]$ implies a possible equilibrium for $p = 0$ at large angles of attack, and

$$p \neq 0 \rightarrow C_l(p) + C_l(p^3) = -\left(\frac{pD}{V}\right) f_1(\delta) - \left(\frac{pD}{V}\right)^3 f_2(\delta) = 0 \tag{20}$$

Equation (20) takes into account the zero average value of the circular components in the wind tunnel. From Eq. (20), $(pD/V) = \pm\sqrt{[-f_1(\delta)]/[f_2(\delta)]}$ implies the two symmetric rates of equilibrium starting at the angle of attack, where $[f_1(\delta)]/[f_2(\delta)] \leq 0$.

The experimental behavior of the rocket when the fin cant is zero is adequately described by the present model by assuming that the solution for $p = 0$ becomes unstable for angles of attack greater than that of the breakout. The numerical application of the method to this case has been carried out using, again, the wing-alone normal-force curve of Fig. 10. The wing-alone normal coefficients defining the curve of Fig. 10 and the weighting factors calculated for the basic finner provide the coefficients of the polynomials $f_1(\delta)$ and $f_2(\delta)$. The result obtained with polynomials up to the fourth order in δ is depicted in Fig. 12, qualitatively reproducing the experimental behavior. The angle of attack where breakout occurs is $\alpha \sim 10°$.

The experimental behavior of the basic finner can also be explained by the bifurcation theory. The roll-moment equation,

$$I_{xx}\dot{p} = qS_wD\left[\left(-\frac{pD}{V}\right) f_1(\delta) + \left(-\frac{pD}{V}\right)^3 f_2(\delta)\right] \tag{21}$$

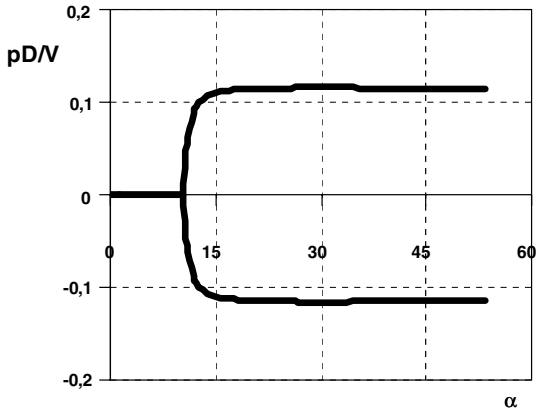

Fig. 12 Steady-state spin vs angle of attack with zero fin cant.

can be rewritten as

$$\dot{P} = P\left[-\frac{f_1(\delta)qS_wD^2}{I_{xx}V}\right] - P^3\left[\frac{f_2(\delta)qS_wD^2}{I_{xx}V}\right] = PA(\delta) - P^3B(\delta) \tag{22}$$

where $P = \frac{pD}{V}$. If, now, the changes $x = P[B(\delta)]^{1/3}$ and $\tau = t[B(\delta)]^{1/3}$ are made, Eq. (22) becomes

$$x' = r(\delta)x - x^3 \tag{23}$$

where $r(\delta) = A(\delta)/[B(\delta)]^{1/3}$, and the prime denotes the derivation with respect to τ. Equation (23) is the normal form of the supercritical pitchfork bifurcation that behaves like the experimental result for the rocket without fin cant. As long as $r(\delta)$ is negative [$f_1(\delta)$ positive and $f_2(\delta)$ negative], the only stable solution is the horizontal axis ($x = P = p = 0$). The bifurcation (breakout) occurs when $r(\delta) = 0$ [$A(\delta) = f_1(\delta) = 0$]. For positive values of $r(\delta)$ [$f_1(\delta)$ and $f_2(\delta)$ negative], the horizontal axis becomes unstable, and two stable symmetric branches depart from the bifurcation point. A fin cant different from zero can be considered an imperfection parameter [15] that breaks the symmetry. If a small fin cant deflection is considered in the present model, the terms in δ_T^2, $\delta_T p^2$, $\delta_T^2 p$, and δ_T^3 of nonzero average can be disregarded. The remaining term in δ_T is the imperfection parameter that makes the system behave as depicted in Fig. 13. The usual pitchfork for no-fin cant disconnects into two pieces. The upper piece is made of stable solutions, whereas the lower piece has stable and unstable branches. The system will usually follow the upper branch as the angle of attack increases, unless a large disturbance makes the stable points of the lower branch accessible.

V. Magnus Side Force

The Magnus force coefficient generated by the four panels in the presence of the body is given by Eq. (E1) of Appendix (E):

$$C_{Yp} = \left(\frac{pD}{V}\right)\left[2C_{N\alpha 0}W^{011}\delta + \frac{9}{2}C_{N\alpha 2}W^{211}\delta^3 + \left(\frac{3}{4}C_{N\alpha 2}W^{031} + \frac{25}{4}C_{N\alpha 4}W^{411}\right)\delta^5 + \frac{75}{16}C_{N\alpha 4}W^{231}\delta^7 + \frac{15}{64}C_{N\alpha 4}W^{051}\delta^9\right] \tag{24}$$

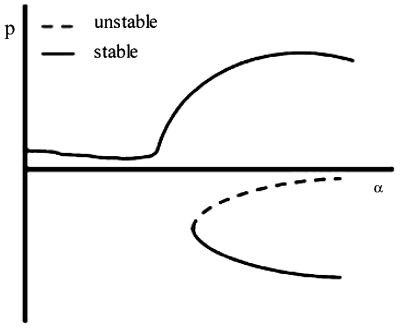

Fig. 13 Steady-state spin vs angle of attack with fin cant.

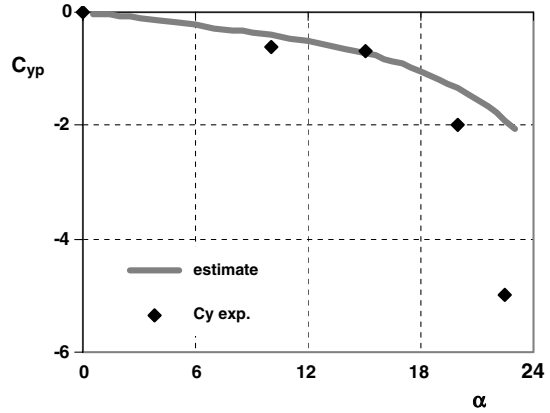

Fig. 15 Magnus side force vs angle of attack (Mach = 0.9).

Assuming that the body Magnus force is negligible [16], the estimate provided by the previous expression can be compared with an experimental result. Reference [17] presents several wind-tunnel results for the basic finner rocket at Mach number 0.9. Unfortunately, the report does not include the wing-alone normal-force coefficients at this Mach number, so they must be extrapolated from the full-normal force and an estimate of the body-alone normal-force curves depicted in Fig. 14.

The curves of Fig. 14 are the least-squares fittings of the experimental data. The difference between the curves is the sum of the wing-body and body-wing components: $C_N - C_{NB} = C_{NwB} + C_{NBw}$. Assuming that the ratio between the wing-body and the body-wing components is equal to the linear ratio ($C_{NwB}/C_{NBw} = C_{NwB}/C_{NBw}|_{\text{linear}}$), the wing-alone coefficients are obtained, and the Magnus side force can be estimated. Figure 15 presents the experimental results of [17] and the estimate given by the present method. The estimate follows the experimental trend and values up to 18° of the angle of attack.

If the Magnus side force is assumed to be applied on the centroid of the wing area, an estimate of the Magnus moment coefficient, with respect to the center of gravity of the rocket, can also be obtained.

VI. Conclusions

This paper presents a strip-SBT application to high incidences to predict the rolling characteristics of cruciform-tailed missiles for which theoretical methods are limited. The SBT, derived from linearized potential theory and, therefore, limited to small angles of attack, does not give accurate estimates in the high-angle-of-attack range, but it is the point of departure for consistent extensions into the nonlinear range of the angles of attack [18,19]. The present approach uses the pattern of interference of the SBT to find the effective angle of attack at every fin station allowing, after expansion in power series, the calculation of the nonlinear rolling derivatives. The resulting rolling derivatives, in addition to the SBT a/b ratio dependence, are functions of the Mach number, AR, and angle of attack. The consistent set of analytical expressions obtained from the method fits the form of the Maple–Synge [4] expansion that is based on the symmetry properties of cruciform configurations and provides a theoretical framework to qualitatively explain the rolling behavior of

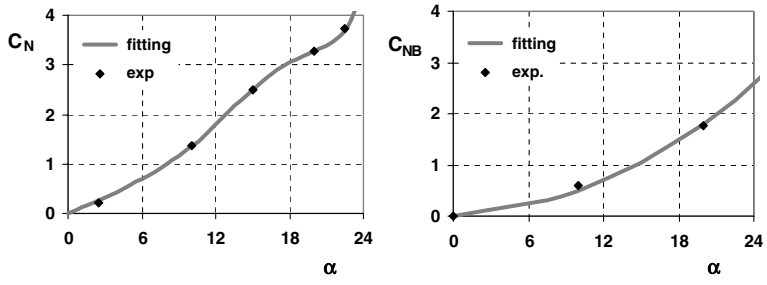

Fig. 14 Normal-force coefficients vs angle of attack (Mach = 0.9).

these configurations [14,20,21]. Regarding its predictive accuracy, direct application of the method through the use of the wing-alone normal-force coefficients obtained by fitting experimental curves is highly dependent on the order of the polynomial used. The best results are usually obtained with the lowest-order polynomial that reasonably represents the nonlinearity of the derivative in the angle-of-attack range of interest (i.e., case of Fig. 10). Better results are obtained when an experimental result is used to extrapolate the behavior of the configuration at a different roll position (i.e., cases of Figs. 4 and 5).

The method is also the only alternative to extrapolate wind-tunnel determinations of rolling derivatives (performed with freedom in roll only) to steady-state free-flight conditions (Appendix D). In addition, the loads on the panels are calculated in the absence of body vortex shedding, making its applicability questionable, particularly at subsonic and transonic Mach numbers for angles of attack greater than 25°, where the separation becomes asymmetric. In general terms, the comparison of the method to the set of experimental results contained in this work shows reasonable agreement up to moderate angles of attack. However, additional wing-alone, and the corresponding wing-body, data are required for further validation to assess the range of applicability of the method.

Appendix A: Wing-Normal-Force Derivation

The normal-force coefficient generated by the four panels up to the seventh order in δ, projected in the crossflow direction indicated by δ (Fig. A1), is

$$
\begin{aligned}
C_{NwB\langle 2\rangle} &= \delta\cos\varphi\Big\{C_{N\alpha 0}\cos\varphi\int_a^b [f+g\delta\sin\varphi]\,\mathrm{d}r \\
&\quad + C_{N\alpha 2}\delta^2\cos^3\varphi\int_a^b [f+g\delta\sin\varphi]^3\,\mathrm{d}r \\
&\quad + C_{N\alpha 4}\delta^4\cos^5\varphi\int_a^b [f+g\delta\sin\varphi]^5\,\mathrm{d}r \\
&\quad + C_{N\alpha 6}\delta^6\cos^7\varphi\int_a^b [f+g\delta\sin\varphi]^7\,\mathrm{d}r\Big\} \\
C_{NwB\langle 4\rangle} &= \delta\cos\varphi\Big\{C_{N\alpha 0}\cos\varphi\int_a^b [f-g\delta\sin\varphi]\,\mathrm{d}r \\
&\quad + C_{N\alpha 2}\delta^2\cos^3\varphi\int_a^b [f-g\delta\sin\varphi]^3\,\mathrm{d}r \\
&\quad + C_{N\alpha 4}\delta^4\cos^5\varphi\int_a^b [f-g\delta\sin\varphi]^5\,\mathrm{d}r \\
&\quad + C_{N\alpha 6}\delta^6\cos^7\varphi\int_a^b [f-g\delta\sin\varphi]^7\,\mathrm{d}r\Big\} \\
C_{NwB\langle 3\rangle} &= \delta\sin\varphi\Big\{C_{N\alpha 0}\sin\varphi\int_a^b [f+g\delta\cos\varphi]\,\mathrm{d}r \\
&\quad + C_{N\alpha 2}\delta^2\sin^3\varphi\int_a^b [f+g\delta\cos\varphi]^3\,\mathrm{d}r \\
&\quad + C_{N\alpha 4}\delta^4\sin^5\varphi\int_a^b [f+g\delta\cos\varphi]^5\,\mathrm{d}r \\
&\quad + C_{N\alpha 6}\delta^6\sin^7\varphi\int_a^b [f+g\delta\cos\varphi]^7\,\mathrm{d}r\Big\} \\
C_{NwB\langle 1\rangle} &= \delta\sin\varphi\Big\{C_{N\alpha 0}\sin\varphi\int_a^b [f-g\delta\cos\varphi]\,\mathrm{d}r \\
&\quad + C_{N\alpha 2}\delta^2\sin^3\varphi\int_a^b [f-g\delta\cos\varphi]^3\,\mathrm{d}r \\
&\quad + C_{N\alpha 4}\delta^4\sin^5\varphi\int_a^b [f-g\delta\cos\varphi]^5\,\mathrm{d}r \\
&\quad + C_{N\alpha 6}\delta^6\sin^7\varphi\int_a^b [f-g\delta\cos\varphi]^7\,\mathrm{d}r\Big\}
\end{aligned}
$$

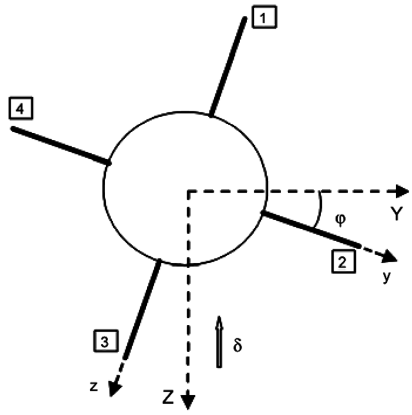

Fig. A1 Wing-normal-force coefficient.

For convenience, the following weighting factors are introduced:

$$W^{nml} = \int_a^b f^n g^m \left(\frac{y}{D}\right)^l \mathrm{d}r \tag{A1}$$

Summing up the contributions of the four panels in each of the wing-alone normal-force coefficients,

$$
\begin{aligned}
C_{N\alpha 0} &\to 2\delta\int_a^b f\,\mathrm{d}r = 2\delta W^{100} \\
C_{N\alpha 2} &\to 2\delta\Big[\delta^2(\sin^4\varphi+\cos^4\varphi)\int_a^b f^3\,\mathrm{d}r \\
&\quad + 3\delta^4(\sin^4\varphi\cos^2\varphi+\cos^4\varphi\sin^2\varphi)\int_a^b fg^2\,\mathrm{d}r\Big] \\
&= 2\delta^3\Big[\frac{1}{4}(3+\cos 4\varphi)W^{300}+\frac{3}{8}(1-\cos 4\varphi)W^{120}\delta^2\Big] \\
C_{N\alpha 4} &\to 2\delta^5\Big[\frac{1}{8}(5+3\cos 4\varphi)W^{500} \\
&\quad + \frac{5}{32}(5-4\cos 4\varphi-\cos 8\varphi)W^{320}\delta^2\Big] \\
C_{N\alpha 6} &\to 2\delta^7\Big[\frac{1}{64}(35+28\cos 4\varphi+\cos 8\varphi)W^{700}\Big]
\end{aligned}
$$

The global wing-normal-force coefficient in the presence of the body is, finally,

$$
\begin{aligned}
C_{NwB} &= 2\delta\{C_{N\alpha 0}W^{100}+\tfrac{3}{4}C_{N\alpha 2}W^{300}\delta^2 \\
&\quad + \tfrac{1}{8}(3C_{N\alpha 2}W^{120}+5C_{N\alpha 4}W^{500})\delta^4 \\
&\quad + \tfrac{1}{64}(50C_{N\alpha 4}W^{320}+35C_{N\alpha 6}W^{700})\delta^6 \\
&\quad + \cos 4\varphi[\tfrac{1}{4}C_{N\alpha 2}W^{300}\delta^2-\tfrac{3}{8}(3C_{N\alpha 2}W^{120}-C_{N\alpha 4}W^{500})\delta^4 \\
&\quad - \tfrac{1}{16}(10C_{N\alpha 4}W^{320}-7C_{N\alpha 6}W^{700})\delta^6] \\
&\quad + \cos 8\varphi[-\tfrac{1}{64}(10C_{N\alpha 4}W^{320}-C_{N\alpha 6}W^{700})\delta^6]\}
\end{aligned}
\tag{A2}
$$

The normal-force coefficient generated by the four panels, projected in the direction of the Y axis of Fig. A1, is the out-of-plane side-force coefficient, which also fits the corresponding Maple–Synge [4] expansion [Eq. (B7) of Appendix B:

$$
\begin{aligned}
C_{YwB} &= \sin 4\varphi[\tfrac{1}{2}C_{N\alpha 2}W^{300}\delta^3+C_{N\alpha 4}W^{500}\delta^5 \\
&\quad + \tfrac{1}{16}(10C_{N\alpha 4}W^{320}+7C_{N\alpha 6}W^{700})\delta^7] \\
&\quad + \sin 8\varphi[-\tfrac{1}{32}(10C_{N\alpha 4}W^{320}-C_{N\alpha 6}W^{700})\delta^7]
\end{aligned}
\tag{A3}
$$

Appendix B: Maple–Synge Expansion

For the case of a symmetric cruciform missile, the in-plane normal force and the static restoring moment are not only functions of the angle of attack but are also dependent on the roll orientation . In addition, the lack of complete axial symmetry introduced by the presence of the fins causes a roll-orientation-dependent side moment and its corresponding side force. Wind-tunnel tests of typical missile configurations [23,24] have shown these side forces and moments to be reasonably described by harmonic functions of the roll-orientation angle. Maple and Synge [4] have shown that symmetry considerations place restrictions on the functional form of the force-and-moment expansion. We can express the force and the roll moment as power series of the complex angle of attack and its conjugate:

$$F = F_y + iF_z = F_y - iN = \sum f_{ij}(V, p, \delta_T)\xi^i\bar{\xi}^j$$

$$L = \sum l_{ij}(V, p, \delta_T)\xi^i\bar{\xi}^j \tag{B1}$$

where $\xi = \delta e^{i\varphi}$ is the complex angle of attack, and the coefficients f_{ij} and l_{ij} are complex functions of the speed of the missile V, the roll rate p, and the fin cant δ_T. Because L is a real variable, $l_{ij} = \bar{l}_{ji}$. The V dependency is generally accounted for through the Mach number not considered here. The rotational symmetry of a cruciform configuration requires that only the following terms are possible up to the eighth order:

$$\begin{aligned} F &= f_{10}\xi + f_{21}\xi^2\bar{\xi} + f_{03}\bar{\xi}^3 + f_{50}\xi^5 + f_{32}\xi^3\bar{\xi}^2 + f_{14}\xi\bar{\xi}^4 \\ &\quad + f_{61}\xi^6\bar{\xi} + f_{43}\xi^4\bar{\xi}^3 + f_{25}\xi^2\bar{\xi}^5 + f_{07}\bar{\xi}^7 \\ L &= l_{00} + l_{11}\xi\bar{\xi} + l_{40}\xi^4 + l_{22}\xi^2\bar{\xi}^2 + l_{04}\bar{\xi}^4 + l_{51}\xi^5\bar{\xi} + l_{33}\xi^3\bar{\xi}^3 \\ &\quad + l_{15}\xi\bar{\xi}^5 + l_{80}\xi^8 + l_{62}\xi^6\bar{\xi}^2 + l_{44}\xi^4\bar{\xi}^4 + l_{26}\xi^2\bar{\xi}^6 + l_{08}\bar{\xi}^8 \end{aligned} \tag{B2}$$

We can further break f_{ij} and l_{ij} down into real and imaginary parts. The mirror symmetry requires them to be even or odd functions in p and δ_T, resulting in

$$f_{ij} = f_{ij}^{(E)} + if_{ij}^{(O)}; \qquad l_{ij} = l_{ij}^{(O)} + il_{ij}^{(E)} \tag{B3}$$

The superscript (E) stands for an even function of p and the superscript (O) for an odd function. If we expand those functions as power series of p and δ_T, we can write

$$\begin{aligned} f_{ij}^E &= f_{ij0} + f_{ij2}\left(\frac{pD}{V}\right)^2 + f_{ij4}\left(\frac{pD}{V}\right)^4 + \cdots \\ f_{ij}^O &= f_{ij1}\frac{pD}{V} + f_{ij3}\left(\frac{pD}{V}\right)^3 + f_{ij5}\left(\frac{pD}{V}\right)^6 + \cdots \\ l_{ij}^O &= l_{ij10}\frac{pD}{V} + l_{ij30}\left(\frac{pD}{V}\right)^3 + \cdots + l_{ij01}\delta_T + l_{ij03}\delta_T^3 + \cdots \\ &\quad + l_{ij21}\left(\frac{pD}{V}\right)^2\delta_T + l_{ij12}\frac{pD}{V}\delta_T^2 + \cdots \\ l_{ij}^E &= l_{ij00} + l_{ij20}\left(\frac{pD}{V}\right)^2 + \cdots + l_{ij02}\delta_T^2 + l_{ij04}\delta_T^4 + \cdots \\ &\quad + l_{ij11}\frac{pD}{V}\delta_T + l_{ij22}\left(\frac{pD}{V}\right)^2\delta_T^2 \cdots \end{aligned} \tag{B4}$$

In the preceding coefficients, the subscripts indicate the powers of ξ, $\bar{\xi}$, pD/V, and δ_T, respectively. The force coefficients f_{ij} are assumed to be independent of δ_T. In the force expansion of Eq. (B2), the roll-dependent terms can be regarded as Magnus terms. The remaining terms, which correspond to coefficients f_{ij0}, yield the following expansion:

$$\begin{aligned} F &= (f_{100} + f_{210}\delta^2 + f_{030}\delta^2 e^{-i4\varphi} + f_{500}\delta^4 e^{i4\varphi} + f_{320}\delta^4 \\ &\quad + f_{140}\delta^4 e^{-i4\varphi} + f_{610}\delta^6 e^{i4\varphi} + f_{430}\delta^6 + f_{250}\delta^6 e^{-i4\varphi} \\ &\quad + f_{070}\delta^6 e^{-i8\varphi})\xi \end{aligned} \tag{B5}$$

Introducing the angle of attack $\xi = i\delta$ (Fig. 2), the complex force F can be broken down into the normal and side forces:

$$\begin{aligned} F_z/\delta = -N/\delta &= f_{100} + f_{210}\delta^2 + f_{320}\delta^4 + f_{430}\delta^6 \\ &\quad + \cos 4\varphi\{f_{030}\delta^2 + (f_{140} + f_{500})\delta^4 + (f_{250} + f_{610})\delta^6\} \\ &\quad + \cos 8\varphi\{f_{070}\delta^6\} \end{aligned} \tag{B6}$$

$$\begin{aligned} F_y/\delta &= \sin 4\varphi\{f_{030}\delta^2 + (f_{140} - f_{500})\delta^4 + (f_{250} - f_{610})\delta^6\} \\ &\quad + \sin 8\varphi\{f_{070}\delta^6\} \end{aligned} \tag{B7}$$

In a similar manner, the Magnus terms can be separated into normal and side contributions. If quadratic and higher powers of roll rate are disregarded, the following expansion is obtained:

$$\begin{aligned} -F_{yp}\Big/\left(\frac{pD}{V}\delta\right) &= f_{101} + f_{211}\delta^2 + f_{321}\delta^4 + f_{431}\delta^6 \\ &\quad + \cos 4\varphi\{f_{031}\delta^2 + (f_{141} + f_{501})\delta^4 + (f_{251} + f_{611})\delta^6\} \\ &\quad + \cos 8\varphi\{f_{071}\delta^6\} \end{aligned} \tag{B8}$$

$$\begin{aligned} N_p\Big/\left(\frac{pD}{V}\delta\right) &= \sin 4\varphi\{f_{031}\delta^2 + (f_{141} - f_{501})\delta^4 \\ &\quad + (f_{251} - f_{611})\delta^6\} + \sin 8\varphi\{f_{071}\delta^6\} \end{aligned} \tag{B9}$$

For the roll moment, by combining the roll expressions of Eqs. (B2) and (B3) and the equality $l_{ij} = \bar{l}_{ji}$,

$$\begin{aligned} L &= l_{00}^O + l_{11}^O\delta^2 + l_{22}^O\delta^4 + l_{33}^O\delta^6 + l_{44}^O\delta^8 \\ &\quad + 2(l_{40}^O\delta^4 + l_{51}^O\delta^6 + l_{62}^O\delta^8)\cos 4\varphi + 2l_{80}^O\delta^8\cos 8\varphi \\ &\quad - 2(l_{40}^E\delta^4 + l_{51}^E\delta^6 + l_{62}^E\delta^8)\sin 4\varphi - 2l_{80}^E\delta^8\sin 8\varphi \end{aligned} \tag{B10}$$

Introducing the expansion given by Eq. (B4), independent terms and terms in p and δ_T can be found. Following, terms up to the eighth order are summarized:

1) For odd products of p and δ_T ($i + j$ odd),

$$\begin{aligned} L &= l_{00ij} + l_{11ij}\delta^2 + l_{22ij}\delta^4 + l_{33ij}\delta^6 + l_{44ij}\delta^8 \\ &\quad + 2(l_{40ij}\delta^4 + l_{51ij}\delta^6 + l_{62ij}\delta^8)\cos 4\varphi \\ &\quad + 2(l_{80ij}\delta^8)\cos 8\varphi \end{aligned} \tag{B11}$$

2) For independent terms and even products of p and δ_T ($i + j$ even),

$$L = -2(l_{40ij}\delta^4 + l_{51ij}\delta^6 + l_{62ij}\delta^8)\sin 4\varphi - 2(l_{80ij}\delta^8)\sin 8\varphi \tag{B12}$$

Appendix C: Weighting Factors

The analytical expressions of the aerodynamic derivatives provided by the present method are functions of the wing-alone normal-force coefficients and the weighting factors, defined by

Table C1 Weighting factors.

λ	0.1	0.2	0.3	0.4	0.5	0.6	0.7	0.8	0.9
w^{100}	5.3×10^{-1}	5.8×10^{-1}	6.2×10^{-1}	6.7×10^{-1}	7.2×10^{-1}	7.7×10^{-1}	8.3×10^{-1}	8.8×10^{-1}	9.4×10^{-1}
w^{300}	6.2×10^{1}	1.6×10^{1}	6.7×10^{0}	3.5×10^{0}	1.9×10^{0}	1.0×10^{0}	5.2×10^{-1}	2.1×10^{-1}	5.0×10^{-2}
w^{120}	1.6×10^{2}	4.4×10^{1}	1.9×10^{1}	9.5×10^{0}	4.8×10^{0}	2.2×10^{0}	8.6×10^{1}	2.4×10^{-1}	2.9×10^{-2}
w^{500}	8.1×10^{3}	4.7×10^{2}	8.0×10^{1}	2.0×10^{1}	5.6×10^{0}	1.6×10^{0}	3.6×10^{-1}	5.8×10^{-2}	3.0×10^{-3}
w^{320}	1.7×10^{4}	1.1×10^{3}	1.9×10^{2}	4.6×10^{1}	1.2×10^{1}	2.7×10^{0}	4.8×10^{-1}	5.1×10^{-2}	1.3×10^{-3}
w^{700}	1.1×10^{6}	1.5×10^{4}	1.0×10^{3}	1.2×10^{2}	1.8×10^{1}	2.5×10^{0}	2.7×10^{-1}	1.6×10^{-2}	1.9×10^{-4}
w^{011}	2.6×10^{0}	1.6×10^{0}	1.2×10^{0}	1.0×10^{0}	9.1×10^{-1}	8.0×10^{-1}	6.8×10^{-1}	5.6×10^{-1}	3.9×10^{-1}
w^{211}	2.2×10^{2}	3.2×10^{1}	1.0×10^{1}	4.2×10^{0}	1.9×10^{0}	8.6×10^{-1}	3.4×10^{-1}	1.1×10^{-1}	1.7×10^{-2}
w^{031}	9.1×10^{2}	1.3×10^{2}	4.3×10^{1}	1.7×10^{1}	7.2×10^{0}	2.8×10^{0}	9.0×10^{-1}	2.0×10^{-1}	1.6×10^{-2}
w^{411}	2.3×10^{4}	8.0×10^{2}	1.0×10^{2}	2.1×10^{1}	4.8×10^{0}	1.1×10^{0}	2.1×10^{-1}	2.5×10^{-2}	8.8×10^{-4}
w^{231}	8.2×10^{4}	2.9×10^{3}	3.8×10^{2}	7.3×10^{1}	1.6×10^{1}	3.0×10^{0}	4.5×10^{-1}	3.8×10^{-2}	6.8×10^{-4}
w^{051}	3.5×10^{5}	1.3×10^{4}	1.7×10^{3}	3.2×10^{2}	6.3×10^{1}	1.1×10^{1}	1.4×10^{0}	8.3×10^{-2}	8.0×10^{-4}
w^{101}	1.3×10^{0}	7.7×10^{-1}	6.1×10^{-1}	5.4×10^{-1}	5.1×10^{-1}	4.9×10^{-1}	4.9×10^{-1}	4.9×10^{-1}	4.9×10^{-1}
w^{301}	1.2×10^{2}	1.8×10^{1}	5.9×10^{0}	2.6×10^{0}	1.3×10^{0}	6.3×10^{-1}	2.9×10^{-1}	1.2×10^{-1}	2.6×10^{-2}
w^{121}	4.3×10^{2}	6.4×10^{1}	2.0×10^{1}	8.2×10^{0}	3.6×10^{0}	1.5×10^{0}	5.3×10^{-1}	1.4×10^{-1}	1.5×10^{-2}
w^{501}	1.4×10^{4}	4.9×10^{2}	6.6×10^{1}	1.4×10^{1}	3.6×10^{0}	9.2×10^{-1}	2.0×10^{-1}	3.1×10^{-2}	1.5×10^{-3}
w^{321}	4.2×10^{4}	1.5×10^{3}	1.9×10^{2}	3.7×10^{1}	8.3×10^{0}	1.7×10^{0}	2.9×10^{-1}	2.9×10^{-2}	7.2×10^{-4}
w^{701}	1.8×10^{6}	1.5×10^{4}	8.0×10^{2}	8.3×10^{1}	1.1×10^{1}	1.4×10^{0}	1.5×10^{-1}	8.8×10^{-3}	9.8×10^{-5}
w^{141}	1.7×10^{5}	6.0×10^{4}	7.8×10^{2}	1.5×10^{2}	3.1×10^{1}	5.7×10^{0}	7.7×10^{-1}	5.4×10^{-2}	7.2×10^{-4}
w^{521}	4.5×10^{6}	3.6×10^{4}	2.0×10^{3}	1.9×10^{2}	2.1×10^{1}	2.3×10^{0}	1.7×10^{-1}	6.7×10^{-3}	3.6×10^{-5}
w^{102}	3.9×10^{0}	1.2×10^{0}	6.6×10^{-1}	4.7×10^{-1}	3.7×10^{-1}	3.2×10^{-1}	2.9×10^{-1}	2.7×10^{-1}	2.6×10^{-1}
w^{302}	3.1×10^{2}	2.4×10^{1}	5.6×10^{0}	2.0×10^{0}	8.5×10^{-1}	3.9×10^{-1}	1.7×10^{-1}	6.3×10^{-2}	1.4×10^{-2}
w^{122}	1.3×10^{3}	1.0×10^{2}	2.3×10^{1}	7.3×10^{0}	2.7×10^{0}	1.0×10^{0}	3.2×10^{-1}	7.9×10^{-2}	8.3×10^{-3}
w^{502}	3.2×10^{4}	5.9×10^{2}	5.8×10^{1}	1.0×10^{1}	2.3×10^{0}	5.5×10^{-1}	1.1×10^{-1}	1.7×10^{-2}	8.0×10^{-4}
w^{322}	1.2×10^{5}	2.1×10^{3}	2.0×10^{2}	3.1×10^{1}	6.1×10^{0}	1.1×10^{0}	1.7×10^{-1}	1.6×10^{-2}	3.8×10^{-4}
w^{702}	3.6×10^{6}	1.6×10^{4}	6.6×10^{2}	5.8×10^{1}	6.9×10^{0}	8.4×10^{-1}	8.0×10^{-2}	4.6×10^{-3}	5.0×10^{-5}
w^{142}	5.1×10^{5}	9.5×10^{3}	8.7×10^{2}	1.3×10^{2}	2.4×10^{1}	3.9×10^{0}	4.7×10^{-1}	3.1×10^{-2}	3.8×10^{-4}
w^{522}	1.2×10^{7}	5.2×10^{4}	1.9×10^{3}	1.5×10^{2}	1.5×10^{1}	1.5×10^{0}	1.0×10^{-1}	3.7×10^{-3}	1.9×10^{-5}
w^{611}	2.7×10^{6}	2.2×10^{4}	1.2×10^{3}	1.1×10^{2}	1.4×10^{1}	1.6×10^{0}	1.3×10^{-1}	6.4×10^{-3}	4.9×10^{-5}
w^{304}	2.9×10^{3}	5.8×10^{1}	6.4×10^{0}	1.4×10^{0}	4.3×10^{-1}	1.5×10^{-1}	5.0×10^{-2}	1.9×10^{-2}	3.7×10^{-3}
w^{124}	1.5×10^{4}	3.0×10^{2}	3.2×10^{1}	6.3×10^{0}	1.7×10^{0}	4.7×10^{-1}	1.2×10^{-1}	2.6×10^{-2}	2.4×10^{-3}
w^{504}	2.4×10^{5}	1.2×10^{3}	5.5×10^{1}	6.3×10^{0}	1.1×10^{0}	2.0×10^{-1}	3.0×10^{-2}	4.8×10^{-3}	2.1×10^{-4}
w^{324}	1.1×10^{6}	5.3×10^{3}	2.4×10^{2}	2.4×10^{1}	3.4×10^{0}	5.0×10^{-1}	6.0×10^{-2}	5.1×10^{-3}	1.0×10^{-4}
w^{704}	2.2×10^{7}	2.7×10^{4}	5.5×10^{2}	3.2×10^{1}	2.9×10^{0}	3.0×10^{1}	2.0×10^{-2}	1.3×10^{-3}	1.3×10^{-5}
w^{144}	5.7×10^{6}	2.7×10^{4}	1.2×10^{3}	1.1×10^{2}	1.4×10^{1}	1.8×10^{0}	1.8×10^{-1}	1.0×10^{-2}	1.0×10^{-4}
w^{524}	9.5×10^{7}	1.1×10^{5}	2.1×10^{3}	1.1×10^{2}	7.9×10^{0}	6.1×10^{-1}	3.0×10^{-2}	1.1×10^{-3}	5.3×10^{-6}
w^{344}	4.5×10^{8}	5.2×10^{5}	9.6×10^{3}	4.6×10^{2}	3.0×10^{1}	2.0×10^{0}	9.0×10^{-2}	2.0×10^{-3}	4.7×10^{-6}
w^{051}	3.5×10^{5}	1.3×10^{4}	1.7×10^{3}	3.2×10^{2}	6.3×10^{1}	1.1×10^{1}	1.4×10^{0}	8.3×10^{-2}	8.0×10^{-4}
w^{431}	8.3×10^{6}	7.2×10^{4}	3.8×10^{3}	3.5×10^{2}	3.8×10^{1}	3.7×10^{0}	2.6×10^{-1}	8.2×10^{-3}	3.2×10^{-5}
w^{032}	2.9×10^{3}	2.2×10^{2}	5.0×10^{1}	1.6×10^{1}	5.6×10^{0}	1.9×10^{0}	5.6×10^{-1}	1.2×10^{-1}	8.8×10^{-3}
w^{412}	5.8×10^{4}	1.1×10^{3}	1.0×10^{2}	1.7×10^{1}	3.4×10^{0}	7.0×10^{-1}	1.2×10^{-1}	1.4×10^{-2}	4.6×10^{-4}
w^{612}	6.2×10^{6}	2.8×10^{4}	1.1×10^{3}	8.6×10^{1}	9.2×10^{0}	9.7×10^{-1}	8.0×10^{-2}	3.5×10^{-3}	2.5×10^{-5}
w^{052}	1.1×10^{6}	2.1×10^{4}	1.9×10^{3}	2.9×10^{2}	4.9×10^{1}	7.6×10^{0}	8.5×10^{-1}	4.7×10^{-2}	4.3×10^{-4}
w^{432}	2.3×10^{7}	1.0×10^{5}	3.8×10^{3}	2.9×10^{2}	2.8×10^{1}	2.5×10^{0}	1.5×10^{-1}	4.6×10^{-3}	1.7×10^{-5}
w^{033}	1.0×10^{4}	3.9×10^{2}	5.9×10^{1}	1.5×10^{1}	4.5×10^{0}	1.3×10^{0}	3.5×10^{-1}	6.7×10^{-2}	4.7×10^{-3}
w^{413}	1.6×10^{5}	1.5×10^{3}	1.0×10^{2}	1.4×10^{1}	2.4×10^{0}	4.5×10^{-1}	7.0×10^{-2}	7.7×10^{-3}	2.4×10^{-4}
w^{613}	1.6×10^{7}	3.7×10^{4}	1.0×10^{3}	6.8×10^{1}	6.3×10^{0}	6.1×10^{-1}	4.0×10^{-2}	1.9×10^{-3}	1.3×10^{-5}
w^{053}	3.8×10^{6}	3.6×10^{4}	2.3×10^{3}	2.7×10^{2}	3.9×10^{1}	5.3×10^{0}	5.3×10^{-1}	2.7×10^{-2}	2.3×10^{-4}
w^{433}	6.6×10^{7}	1.5×10^{5}	4.1×10^{3}	2.5×10^{2}	2.0×10^{1}	1.6×10^{0}	9.0×10^{-2}	2.6×10^{-3}	9.0×10^{-6}
w^{303}	9.1×10^{2}	3.5×10^{1}	5.8×10^{0}	1.6×10^{0}	6.0×10^{-1}	2.4×10^{-1}	1.0×10^{-1}	3.4×10^{-2}	7.0×10^{-3}
w^{123}	4.4×10^{3}	1.7×10^{2}	2.6×10^{1}	6.7×10^{0}	2.1×10^{0}	6.8×10^{-1}	2.0×10^{-1}	4.5×10^{-2}	4.4×10^{-3}
w^{503}	8.2×10^{4}	7.9×10^{2}	5.5×10^{1}	7.9×10^{0}	1.6×10^{0}	3.3×10^{-1}	6.0×10^{-2}	8.9×10^{-3}	4.1×10^{-4}
w^{323}	3.5×10^{5}	3.3×10^{3}	2.1×10^{2}	2.7×10^{1}	4.5×10^{0}	7.5×10^{-1}	1.0×10^{-1}	9.1×10^{-3}	2.0×10^{-4}
w^{703}	8.4×10^{6}	2×10^{4}	5.8×10^{2}	4.2×10^{1}	4.5×10^{0}	5.0×10^{-1}	4.0×10^{-2}	2.5×10^{-3}	2.6×10^{-5}
w^{143}	1.7×10^{6}	1.6×10^{4}	1.0×10^{3}	1.2×10^{2}	1.8×10^{1}	2.7×10^{0}	2.9×10^{-1}	1.8×10^{-2}	2.0×10^{-4}
w^{523}	3.2×10^{7}	7.4×10^{4}	2.0×10^{3}	1.3×10^{2}	1.0×10^{1}	9.4×10^{-1}	6.0×10^{-2}	2.0×10^{-3}	1.0×10^{-5}
w^{343}	1.4×10^{8}	3.2×10^{5}	8.5×10^{3}	5.1×10^{2}	4.0×10^{1}	2.9×10^{0}	1.5×10^{-1}	3.5×10^{-3}	8.9×10^{-6}
w^{342}	4.6×10^{7}	2.1×10^{5}	7.8×10^{3}	5.9×10^{2}	5.3×10^{1}	4.4×10^{0}	2.5×10^{-1}	6.2×10^{-2}	1.6×10^{-5}
w^{341}	1.6×10^{7}	1.4×10^{5}	7.4×10^{3}	6.8×10^{2}	7.1×10^{1}	6.6×10^{0}	4.1×10^{-1}	1.1×10^{-2}	3.1×10^{-5}

$$
\begin{aligned}
W^{nml} &= \int_a^b f^n g^m \left(\frac{y}{D}\right)^l \mathrm{d}r \\
&= \int_a^b \frac{4^n}{C^n_{N\alpha w 0sbt} D^n} \left[\left(b+\frac{a^2}{b}\right)^2 - \left(y+\frac{a^2}{y}\right)^2\right]^{n/2} \\
&\times \frac{4^m (2)^{\frac{m}{2}} [y^4 - a^4]^{3m/2}}{AR^m y^{5m} C^m_{N\alpha w 0\mathrm{sbt}} D^m} [F(\psi_1, k) + F(\psi_2, k')]^m \left(\frac{y}{D}\right)^l \frac{D\mathrm{d}y}{S_w} \\
&= \frac{2^{2n+(5/2)m}}{AR^m C^{n+m}_{N\alpha w 0\mathrm{sbt}} D^{n+m+l-1} S_w} \\
&\times \int_a^b \left\{ \left[\left(b+\frac{a^2}{b}\right)^2 - \left(y+\frac{a^2}{y}\right)^2\right]^{n/2} \frac{[y^4 - a^4]^{3m/2}}{y^{5m-l}} \right. \\
&\left. \times [F(\psi_1, k) + F(\psi_2, k')]^m \right\} \mathrm{d}y
\end{aligned}
$$

The preceding expression implies

$$
\begin{aligned}
W^{nml} &= \frac{\lambda^2}{AR^{n+2m-1} 2^{(5/2)m} \pi^{n+m} (1-\lambda)^2} \int_{1/2}^{1/2\lambda} \left\{ \left[\left(\frac{2\lambda^2+2}{\lambda}\right)^2 \right.\right. \\
&\left.\left. - \left(\frac{4z^2+1}{z}\right)^2 \right]^{n/2} \frac{[16z^4-1]^{3m/2}}{z^{5m-l}} [F(\psi_1, k) + F(\psi_2, k')]^m \right\} \mathrm{d}z; \\
z &= \frac{y}{D}; \qquad \lambda = \frac{a}{b} = \frac{D}{2b}
\end{aligned}
$$

The weighting factors for $AR = 1$ (w^{nml}) can be evaluated as a function of λ only and are listed in Table C1. For arbitrary AR, the corresponding weighting factor is

$$W^{nml} = w^{nml}/AR^{n+2m-1}$$

Appendix D: Roll Derivatives

If the four panels are deflected to generate a positive rolling moment (Fig. D1), the ratio of the unperturbed normal velocity to missile velocity on the strips of panel 2 is

$$\frac{V_n}{V} = \delta\cos\varphi - \delta_T + \frac{py}{V} = \delta\cos\varphi - \Delta$$

The differential roll-moment coefficient generated by two strips situated at distance y from the body center on panels 2 and 4 is:

$$
\begin{aligned}
dC_{l\langle 2-4\rangle} &= \tfrac{y}{D}\mathrm{d}r\{-C_{N\alpha 0}[\delta\cos\varphi - \Delta](f + g\delta\sin\varphi) \\
&- C_{N\alpha 2}[\delta\cos\varphi - \Delta]^3 (f + g\delta\sin\varphi)^3 \\
&- C_{N\alpha 4}[\delta\cos\varphi - \Delta]^5 (f + g\delta\sin\varphi)^5 - C_{N\alpha 6}[\delta\cos\varphi - \Delta]^7 \\
&\times (f + g\delta\sin\varphi)^7\} + \tfrac{y}{D}\mathrm{d}r\{C_{N\alpha 0}[\delta\cos\varphi + \Delta](f - g\delta\sin\varphi) \\
&+ C_{N\alpha 2}[\delta\cos\varphi + \Delta]^3 (f - g\delta\sin\varphi)^3 + C_{N\alpha 4}[\delta\cos\varphi + \Delta]^5 \\
&\times (f - g\delta\sin\varphi)^5 + C_{N\alpha 6}[\delta\cos\varphi + \Delta]^7 (f - g\delta\sin\varphi)^7\}
\end{aligned}
$$

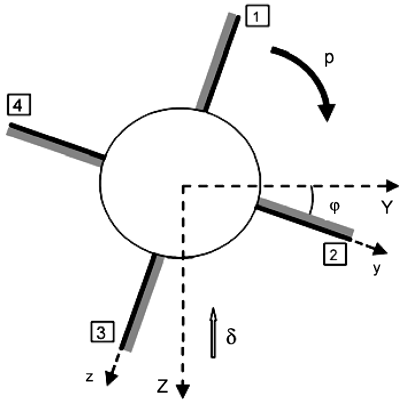

Fig. D1 Rolling moment.

Similarly, for panels 3 and 1,

$$
\begin{aligned}
dC_{l\langle 3-1\rangle} &= \tfrac{y}{D}\mathrm{d}r\{C_{N\alpha 0}[\delta\sin\varphi + \Delta](f + g\delta\cos\varphi) \\
&+ C_{N\alpha 2}[\delta\sin\varphi + \Delta]^3 (f + g\delta\cos\varphi)^3 + C_{N\alpha 4}[\delta\sin\varphi + \Delta]^5 \\
&\times (f + g\delta\cos\varphi)^5 + C_{N\alpha 6}[\delta\sin\varphi + \Delta]^7 (f + g\delta\cos\varphi)^7\} \\
&+ \tfrac{y}{D}\mathrm{d}r\{-C_{N\alpha 0}[\delta\sin\varphi - \Delta](f - g\delta\cos\varphi) \\
&- C_{N\alpha 2}[\delta\sin\varphi - \Delta]^3 (f - g\delta\cos\varphi)^3 - C_{N\alpha 4}[\delta\sin\varphi - \Delta]^5 \\
&\times (f - g\delta\cos\varphi)^5 - C_{N\alpha 6}[\delta\sin\varphi - \Delta]^7 (f - g\delta\cos\varphi)^7\}
\end{aligned}
$$

Summing up the contributions in each of the wing-alone normal-force coefficients,

$$
\begin{aligned}
C_{N\alpha 0} &\to (\tfrac{y}{D})\mathrm{d}r 4f\Delta; \\
C_{N\alpha 2} &\to (\tfrac{y}{D})\mathrm{d}r[4f^3\Delta^3 + 6fg^2\Delta^3\delta^2 \\
&- 6f^2 g\sin\varphi\cos\varphi(\cos^2\varphi - \sin^2\varphi)\delta^4 + 6f^3\Delta\delta^2 \\
&+ 36fg^2\sin^2\varphi\cos^2\varphi\Delta\delta^4 \\
&- 6g^3\sin\varphi\cos\varphi(\sin^2\varphi - \cos^2\varphi)\Delta^2\delta^4] \\
&= (\tfrac{y}{D})\mathrm{d}r[4f^3\Delta^3 + 6fg^2\Delta^3\delta^2 - \tfrac{3}{2}f^2 g\sin 4\varphi\delta^4 + 6f^3\Delta\delta^2 \\
&+ \tfrac{9}{2}fg^2(1-\cos 4\varphi)\Delta\delta^4 + \tfrac{3}{2}g^3\sin 4\varphi\Delta^2\delta^4] \\
C_{N\alpha 4} &\to (\tfrac{y}{D})\mathrm{d}r[-\tfrac{5}{2}f^4 g\sin 4\varphi\delta^6 - \tfrac{5}{16}f^2 g^3(2\sin 4\varphi - \sin 8\varphi)\delta^8 \\
&+ 20f^5\Delta^3\delta^2 + 50f^3 g^2(1-\cos 4\varphi)\Delta^3\delta^4 \\
&+ \tfrac{25}{2}fg^4(1-\cos 4\varphi)\Delta^3\delta^6 - \tfrac{5}{16}g^5(2\sin 4\varphi - \sin 8\varphi)\Delta^2\delta^8 \\
&- 2f^4 g\sin 4\varphi\Delta^2\delta^4 + \tfrac{5}{2}f^5(3+\cos 4\varphi)\Delta\delta^4 \\
&+ \tfrac{25}{2}f^3 g^2(1-\cos 4\varphi)\Delta\delta^6 + \tfrac{25}{32}fg^4(3-4\cos 4\varphi + \cos 8\varphi)\Delta\delta^8] \\
C_{N\alpha 6} &\to (\tfrac{y}{D})\mathrm{d}r[-\tfrac{7}{32}f^6 g(14\sin 4\varphi + \sin 8\varphi)\delta^8 \\
&- \tfrac{35}{2}f^7(3+\cos 4\varphi)\Delta^3\delta^4 + \tfrac{735}{4}f^5 g^2(1-\cos 4\varphi)\Delta^3\delta^6 \\
&+ \tfrac{1225}{32}f^3 g^4 3(1 - 4\cos 4\varphi + \cos 8\varphi)\Delta^3\delta^8 \\
&- \tfrac{147}{2}f^6 g\sin 4\varphi\Delta^2\delta^6 - \tfrac{735}{32}f^4 g^3(2\sin 4\varphi - \sin 8\varphi)\Delta^2\delta^8 \\
&+ \tfrac{7}{4}f^7 g(5 + 3\cos 4\varphi)\Delta^2\delta^4 + \tfrac{5}{2}f^5(3+\cos 4\varphi)\Delta\delta^4 \\
&+ \tfrac{25}{2}f^3 g^2(1-\cos 4\varphi)\Delta\delta^6 + \tfrac{25}{32}fg^4(3-4\cos 4\varphi + \cos 8\varphi)\Delta\delta^6 \\
&+ \tfrac{147}{32}f^5 g^2(5 - 4\cos 4\varphi - \cos 8\varphi)]
\end{aligned}
$$

Only powers of Δ, up to Δ^3, were retained, taking into account that Δ is smaller than the large values of δ, at which the previous expressions can theoretically be applied. If, now, Δ is replaced by $\delta_T - \frac{py}{V}$, the preceding sums give raise to independent terms and terms in δ_T, p, $\delta_T p$, δ_T^2, p^2, $\delta_T p^2$, $\delta_T^2 p$, δ_T^3, and p^3. The independent term is the induced roll moment, the term in δ_T is the linear roll-driving moment, the term in p is the linear roll-damping moment, and the term in p^3 is the cubic roll-damping moment. The integration along the span yields the aforementioned roll-moment components that fit the corresponding Maple–Synge [4] expansion [Eqs. (B11) and (B12) of Appendix B] and are listed next:

Linear roll-driving moment:

$$
\begin{aligned}
C_l(\delta_T) &= \delta_T\{4C_{N\alpha 0}W^{101} + 6C_{N\alpha 2}W^{301}\delta^2 \\
&+ (\tfrac{9}{2}C_{N\alpha 2}W^{121} + \tfrac{15}{2}C_{N\alpha 4}W^{501})\delta^4 \\
&+ (\tfrac{25}{2}C_{N\alpha 4}W^{321} + \tfrac{35}{4}C_{N\alpha 6}W^{701})\delta^6 \\
&+ (\tfrac{75}{32}C_{N\alpha 4}W^{141} + \tfrac{735}{32}C_{N\alpha 6}W^{521})\delta^8 \\
&+ \cos 4\varphi[(-\tfrac{9}{2}C_{N\alpha 2}W^{121} + \tfrac{5}{2}C_{N\alpha 4}W^{501})\delta^4 \\
&+ (-\tfrac{25}{2}C_{N\alpha 4}W^{321} + \tfrac{21}{4}C_{N\alpha 6}W^{701})\delta^6 \\
&- (\tfrac{25}{8}C_{N\alpha 4}W^{141} + \tfrac{147}{8}C_{N\alpha 6}W^{521})\delta^8] \\
&+ \cos 8\varphi[(\tfrac{25}{32}C_{N\alpha 4}W^{141} - \tfrac{147}{32}C_{N\alpha 6}W^{521})\delta^8]\}
\end{aligned}
\tag{D1}
$$

Linear roll-damping moment:

$$\begin{aligned}C_l(p) = (-\frac{pD}{V})\{&4C_{N\alpha 0}W^{102} + 6C_{N\alpha 2}W^{302}\delta^2\\ &+ (\tfrac{9}{2}C_{N\alpha 2}W^{122} + \tfrac{15}{2}C_{N\alpha 4}W^{502})\delta^4\\ &+ (\tfrac{25}{2}C_{N\alpha 4}W^{322} + \tfrac{35}{4}C_{N\alpha 6}W^{702})\delta^6\\ &+ (\tfrac{75}{32}C_{N\alpha 4}W^{142} + \tfrac{735}{32}C_{N\alpha 6}W^{522})\delta^8\\ &+ \cos 4\varphi[(-\tfrac{9}{2}C_{N\alpha 2}W^{122} + \tfrac{5}{2}C_{N\alpha 4}W^{502})\delta^4\\ &+ (-\tfrac{25}{2}C_{N\alpha 4}W^{322} + \tfrac{21}{4}C_{N\alpha 6}W^{702})\delta^6\\ &- (\tfrac{25}{8}C_{N\alpha 4}W^{142} + \tfrac{147}{8}C_{N\alpha 6}W^{522})\delta^8]\\ &+ \cos 8\varphi[(\tfrac{25}{32}C_{N\alpha 4}W^{142} - \tfrac{147}{32}C_{N\alpha 6}W^{522})\delta^8]\}\end{aligned} \tag{D2}$$

Induced roll moment:

$$\begin{aligned}C_l(\text{ind.}) = \{&\sin 4\varphi[-\tfrac{3}{2}C_{N\alpha 2}W^{211}\delta^4 - \tfrac{5}{2}C_{N\alpha 4}W^{411}\delta^6\\ &- (\tfrac{5}{8}C_{N\alpha 4}W^{231} + \tfrac{49}{16}C_{N\alpha 6}W^{611})\delta^8]\\ &+ \sin 8\varphi[(\tfrac{5}{16}C_{N\alpha 4}W^{231} - \tfrac{7}{32}C_{N\alpha 6}W^{611})\delta^8]\}\end{aligned} \tag{D3}$$

Cubic roll-damping moment:

$$\begin{aligned}C_l(p^3) = (-\tfrac{pD}{V})^3\{&4C_{N\alpha 2}W^{304} + (6C_{N\alpha 2}W^{124} + 20C_{N\alpha 4}W^{504})\delta^2\\ &+ (50C_{N\alpha 4}W^{324} + \tfrac{105}{2}C_{N\alpha 6}W^{704})\delta^4\\ &+ (\tfrac{25}{2}C_{N\alpha 4}W^{144} + \tfrac{735}{4}C_{N\alpha 6}W^{524})\delta^6 + (\tfrac{3675}{32}C_{N\alpha 6}W^{344})\delta^8\\ &+ \cos 4\varphi[(-50C_{N\alpha 4}W^{324} + \tfrac{35}{2}C_{N\alpha 6}W^{704})\delta^4\\ &- (\tfrac{25}{2}C_{N\alpha 4}W^{144} + \tfrac{735}{4}C_{N\alpha 6}W^{524})\delta^6 - (\tfrac{1225}{8}C_{N\alpha 6}W^{344})\delta^8]\\ &+ \cos 8\varphi[(\tfrac{1225}{32}C_{N\alpha 6}W^{344})\delta^8]\}\end{aligned} \tag{D4}$$

$$\begin{aligned}C_l(\delta_T^2) = \delta_T^2\{&\sin 4\varphi[(\tfrac{3}{2}C_{N\alpha 2}W^{031} - 25C_{N\alpha 4}W^{411})\delta^4\\ &- (\tfrac{147}{2}C_{N\alpha 6}W^{611})\delta^6 + (\tfrac{5}{8}C_{N\alpha 4}W^{051} - \tfrac{735}{16}C_{N\alpha 6}W^{431})\delta^8]\\ &+ \sin 8\varphi[(-\tfrac{5}{16}C_{N\alpha 4}W^{051} + \tfrac{735}{32}C_{N\alpha 6}W^{431})\delta^8]\}\end{aligned} \tag{D5}$$

$$\begin{aligned}C_l(\delta_T p) = 2\delta_T(-\tfrac{pD}{V})\{&\sin 4\varphi[(\tfrac{3}{2}C_{N\alpha 2}W^{032} - 25C_{N\alpha 4}W^{412})\delta^4\\ &- (\tfrac{147}{2}C_{N\alpha 6}W^{612})\delta^6 + (\tfrac{5}{8}C_{N\alpha 4}W^{052} - \tfrac{735}{16}C_{N\alpha 6}W^{432})\delta^8]\\ &+ \sin 8\varphi[(-\tfrac{5}{16}C_{N\alpha 4}W^{052} + \tfrac{735}{32}C_{N\alpha 6}W^{432})\delta^8]\}\end{aligned} \tag{D6}$$

$$\begin{aligned}C_l(p^2) = (\tfrac{pD}{V})^2\{&\sin 4\varphi[(\tfrac{3}{2}C_{N\alpha 2}W^{033} - 25C_{N\alpha 4}W^{413})\delta^4\\ &- (\tfrac{147}{2}C_{N\alpha 6}W^{613})\delta^6 + (\tfrac{5}{8}C_{N\alpha 4}W^{053} - \tfrac{735}{16}C_{N\alpha 6}W^{433})\delta^8]\\ &+ \sin 8\varphi[(-\tfrac{5}{16}C_{N\alpha 4}W^{053} + \tfrac{735}{32}C_{N\alpha 6}W^{433})\delta^8]\}\end{aligned} \tag{D7}$$

$$\begin{aligned}C_l(\delta_T p^2) = 3\delta_T(\tfrac{pD}{V})^2\{&4C_{N\alpha 2}W^{303}\\ &+ (6C_{N\alpha 2}W^{123} + 20C_{N\alpha 4}W^{503})\delta^2\\ &+ (50C_{N\alpha 4}W^{323} + \tfrac{105}{2}C_{N\alpha 6}W^{703})\delta^4\\ &+ (\tfrac{25}{2}C_{N\alpha 4}W^{143} + \tfrac{735}{4}C_{N\alpha 6}W^{523})\delta^6 + (\tfrac{3675}{32}C_{N\alpha 6}W^{343})\delta^8\\ &+ \cos 4\varphi[(-50C_{N\alpha 4}W^{323} + \tfrac{35}{2}C_{N\alpha 6}W^{703})\delta^4\\ &- (\tfrac{25}{2}C_{N\alpha 4}W^{143} + \tfrac{735}{4}C_{N\alpha 6}W^{523})\delta^6 - (\tfrac{1225}{8}C_{N\alpha 6}W^{343})\delta^8]\\ &+ \cos 8\varphi[(\tfrac{1225}{32}C_{N\alpha 6}W^{343})\delta^8]\}\end{aligned} \tag{D8}$$

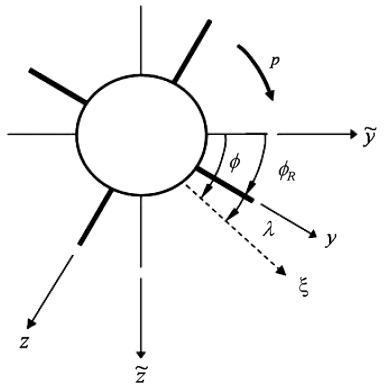

Fig. D2 Circular motion.

$$\begin{aligned}C_l(\delta_T^2 p) = 3\delta_T^2(-\tfrac{pD}{V})\{&4C_{N\alpha 2}W^{302}\\ &+ (6C_{N\alpha 2}W^{122} + 20C_{N\alpha 4}W^{502})\delta^2\\ &+ (50C_{N\alpha 4}W^{322} + \tfrac{105}{2}C_{N\alpha 6}W^{702})\delta^4\\ &+ (\tfrac{25}{2}C_{N\alpha 4}W^{142} + \tfrac{735}{4}C_{N\alpha 6}W^{522})\delta^6 + (\tfrac{3675}{32}C_{N\alpha 6}W^{342})\delta^8\\ &+ \cos 4\varphi[(-50C_{N\alpha 4}W^{322} + \tfrac{35}{2}C_{N\alpha 6}W^{702})\delta^4\\ &- (\tfrac{25}{2}C_{N\alpha 4}W^{142} + \tfrac{735}{4}C_{N\alpha 6}W^{522})\delta^6 - (\tfrac{1225}{8}C_{N\alpha 6}W^{342})\delta^8]\\ &+ \cos 8\varphi[(\tfrac{1225}{32}C_{N\alpha 6}W^{342})\delta^8]\}\end{aligned} \tag{D9}$$

$$\begin{aligned}C_l(\delta_T^3) = \delta_T^3\Bigg\{&4C_{N\alpha 2}W^{301} + (6C_{N\alpha 2}W^{121} + 20C_{N\alpha 4}W^{501})\delta^2\\ &+ \left(50C_{N\alpha 4}W^{321} + \frac{105}{2}C_{N\alpha 6}W^{701}\right)\delta^4\\ &+ \left(\frac{25}{2}C_{N\alpha 4}W^{141} + \frac{735}{4}C_{N\alpha 6}W^{521}\right)\delta^6\\ &+ \left(\frac{3675}{32}C_{N\alpha 6}W^{341}\right)\delta^8\\ &+ \cos 4\varphi\left[\left(\frac{35}{2}C_{N\alpha 6}W^{701} - 50C_{N\alpha 4}W^{321}\right)\delta^4\right.\\ &- \left(\frac{25}{2}C_{N\alpha 4}W^{141} + \frac{735}{4}C_{N\alpha 6}W^{521}\right)\delta^6\\ &\left.- \left(\frac{1225}{8}C_{N\alpha 6}W^{341}\right)\delta^8\right]\\ &+ \cos 8\varphi\left[\left(\frac{1225}{32}C_{N\alpha 6}W^{341}\right)\delta^8\right]\Bigg\}\end{aligned} \tag{D10}$$

The expressions of the preceding roll-moment components can be easily extended to higher orders in the wing-alone coefficients and powers of δ and Δ. According to Fig. D2, $\dot{\phi} = \dot{\phi}_R + \dot{\lambda}$. Since $\lambda + \varphi = 90°$, then $\dot{\phi} = \omega = p - \dot{\varphi}$, where ω is the circular yaw frequency. In lunar motion, $\dot{\lambda} = -\dot{\varphi} = 0 \Rightarrow \omega = p$ and $\varphi =$ constant. For the wind-tunnel case, with freedom only in roll. [11] $\omega = 0 \Rightarrow p = \dot{\varphi}$. In the last case, the contribution of the terms in $\sin 4k\varphi$ and $\cos 4k\varphi$ ($k = 1, 2$) to the roll moment is zero in average; therefore, the terms of the form $p^j \sin 4k\varphi$ and $p^j \cos 4k\varphi$ ($j = 1, 2, 3$) cannot be detected in wind-tunnel tests, because their contributions are always null (when $p = 0$ or $p \neq 0$) but can have influence in free-flight conditions.

Appendix E: Magnus Side-Force Derivation

The Magnus force generated by the wing in the presence of the body has in-plane components of nonzero average in

$(pD/V)^2$, $(pD/V)^4, \cdots$ that can be disregarded in comparison with the in-plane gross components (Sec. III). Assuming that the configuration is rolling at rate p, the calculation of the out-of- plane forces is as follows:

$$C_{YwB\langle 2\rangle} = \sin\varphi\left\{C_{N\alpha 0}\int_a^b [f + g\delta\sin\varphi][\delta\cos\varphi + py/V]\,\mathrm{d}r + C_{N\alpha 2}\int_a^b [f + g\delta\sin\varphi]^3[\delta\cos\varphi + py/V]^3\,\mathrm{d}r + \cdots\right\}$$

$$C_{YwB\langle 4\rangle} = \sin\varphi\left\{C_{N\alpha 0}\int_a^b [f - g\delta\sin\varphi][\delta\cos\varphi - py/V]\,\mathrm{d}r + C_{N\alpha 2}\int_a^b [f - g\delta\sin\varphi]^3[\delta\cos\varphi - py/V]^3\,\mathrm{d}r + \cdots\right\}$$

$$C_{YwB\langle 3\rangle} = -\cos\varphi\left\{C_{N\alpha 0}\int_a^b [f + g\delta\cos\varphi][\delta\sin\varphi - py/V]\,\mathrm{d}r + C_{N\alpha 2}\int_a^b [f + g\delta\cos\varphi]^3[\delta\sin\varphi - py/V]^3\,\mathrm{d}r + \cdots\right\}$$

$$C_{YwB\langle 1\rangle} = -\cos\varphi\left\{C_{N\alpha 0}\int_a^b [f - g\delta\cos\varphi][\delta\sin\varphi + py/V]\,\mathrm{d}r + C_{N\alpha 2}\int_a^b [f - g\delta\cos\varphi]^3[\delta\sin\varphi + py/V]^3\,\mathrm{d}r + \cdots\right\}$$

The partial sums in the wing-alone normal-force coefficients up to $C_{N\alpha 4}$ are

$$C_{N\alpha 0} \to 2\delta\int_a^b g\frac{pD}{V}\frac{y}{D}\,\mathrm{d}r = 2\delta\left(\frac{pD}{V}\right)W^{011};$$

$$\begin{aligned} C_{N\alpha 2} \to &\left[6\delta^5\sin^2\varphi\cos^2\varphi(\sin^2\varphi + \cos^2\varphi)\int_a^b g^3\frac{py}{V}\,\mathrm{d}r\right. \\ &+ 36\delta^3\sin^2\varphi\cos^2\varphi\int_a^b f^2 g\frac{py}{V}\,\mathrm{d}r \\ &\left.- 18\delta^3\sin\varphi\cos\varphi(\cos^2\varphi - \sin^2\varphi)\int_a^b fg^2\left(\frac{py}{V}\right)^2\mathrm{d}r\right] \\ &= \left[6\delta^5\left(\frac{1}{8} - \frac{\cos 4\varphi}{8}\right)\int_a^b g^3\frac{py}{V}\,\mathrm{d}r\right. \\ &+ 36\delta^3\left(\frac{1}{8} - \frac{\cos 4\varphi}{8}\right)\int_a^b f^2 g\frac{py}{V}\,\mathrm{d}r \\ &\left.- 18\delta^3\frac{1}{4}\sin 4\varphi\int_a^b fg^2\left(\frac{py}{V}\right)^2\mathrm{d}r\right] \\ &= \left(\frac{pD}{V}\right)\left(\frac{9}{2}\delta^3 W^{211} + \frac{3}{4}\delta^5 W^{031}\right) \end{aligned}$$

in which the circular terms were disregarded, assuming freedom only in roll. Similarly,

$$C_{N\alpha 4} \to \left(\tfrac{pD}{V}\right)\left(\tfrac{25}{4}\delta^5 W^{411} + \tfrac{75}{16}\delta^7 W^{231} + \tfrac{15}{64}\delta^9 W^{051}\right)$$

and the Magnus side force is, finally,

$$\begin{aligned} C_{Yp} = &\left(\tfrac{pD}{V}\right)[2C_{N\alpha 0}W^{011}\delta + \tfrac{9}{2}C_{N\alpha 2}W^{211}\delta^3 \\ &+ \left(\tfrac{3}{4}C_{N\alpha 2}W^{031} + \tfrac{25}{4}C_{N\alpha 4}W^{411}\right)\delta^5 \\ &+ \tfrac{75}{16}C_{N\alpha 4}W^{231}\delta^7 + \tfrac{15}{64}C_{N\alpha 4}W^{051}\delta^9] \end{aligned} \tag{E1}$$

If a roll deflection is considered in the calculation, the Magnus force due to fin cant can also be found [25,26].

References

[1] Nicolaides, J. D., "Two Non-Linear Problems in the Flight Dynamics of Modern Ballistic Missiles," Inst. of Aeronautical Sciences, Rept. 59-17, New York, 1959.

[2] Nielsen, J. N., *Missile Aerodynamics*, Nielsen Engineering and Research, Mountain View, CA, 1988, Chap. 5.

[3] Moore, F. G., *Approximate Methods for Weapon Aerodynamics*, Vol. 186, Progress in Astronautics and Aeronautics, AIAA, Reston, VA, 2000, Chap. 5.

[4] Maple, C. G., and Synge, J. L., "Aerodynamic Symmetry of Projectiles," *Quarterly of Applied Mathematics*, Vol. 4, Jan. 1949, pp. 345–366.

[5] Meyer, J., "Effects of the Roll Angle on Cruciform Wing-Body Configurations at High Incidences," *Journal of Spacecraft and Rockets*, Vol. 31, No. 1, 1994, pp. 113–122. doi:10.2514/3.26410

[6] Moore, F. G., and Moore, L. Y., "New Method to Predict Nonlinear Roll Damping Moments," *Journal of Spacecraft and Rockets*, Vol. 45, No. 5, 2008, pp. 955–964. doi:10.2514/1.34974

[7] Eastman, D. W., "Roll Damping of Cruciform-Tailed Missiles," *Journal of Spacecraft and Rockets*, Vol. 23, No. 1, 1986, pp. 119–120. doi:10.2514/3.25794

[8] Mikhail, A. G., "Roll Damping for Projectiles Including Wraparound, Offset, and Arbitrary Number of Fins," *Journal of Spacecraft and Rockets*, Vol. 32, No. 6, 1995, pp. 929–937. doi:10.2514/3.26711

[9] Chadwick, W. R., "Flight Dynamics of a Bomb with Cruciform Tail," *Journal of Spacecraft and Rockets*, Vol. 4, No. 6, 1967, pp. 768–773. doi:10.2514/3.28949

[10] Mikhail, A. G., "Fin Damage and Mass Offset for Kinetic Energy Projectile Spin/Pitch Lock-In," *Journal of Spacecraft and Rockets*, Vol. 35, No. 3, 1998, pp. 287–295. doi:10.2514/2.3353

[11] Oberkampf, W. L., and Nicolaides, J. D., "Aerodynamics of Finned Missiles at High Angle of Attack," *AIAA Journal*, Vol. 9, No. 12, 1971, pp. 2378–2384. doi:10.2514/3.50043

[12] Winter, H., "Flow Phenomena on Plates and Airfoils of Short Span," NASA TM 798, 1937.

[13] Moore, F. G., and Hymer, T., "2005 Version of the Aeroprediction Code (AP05)," *Journal of Spacecraft and Rockets*, Vol. 42,, No. 2, 2005, pp. 240–256. doi:10.2514/1.7970

[14] Daniels, P., "A Study of the Nonlinear Rolling Motion of a Four-Finned Missile," *Journal of Spacecraft and Rockets*, Vol. 7, No. 4, 1970, pp. 510–512. doi:10.2514/3.29982

[15] Strogatz, S. H., *Nonlinear Dynamics and Chaos*, Perseus Books Publ., Cambridge, England, U.K., 1994, Chap. 3.

[16] Murphy, C. H., "Free Flight Motion of Symmetric Missiles," U.S. Army Ballistic Research Lab. Rept. 1216, Aberdeen Proving Ground, MD, March 1963, p. 134.

[17] Collins, J. A., "Verification Test of the AEDC High Alpha Roll Dynamics System," U.S. Air Force, Arnold Engineering Development Center Rept. TSR-78-P50, Arnold, AFB, TN, 1978.

[18] Hemsch, M. J., and Nielsen, J. N., "Equivalent Angle-of-Attack Method for Estimating Nonlinear Aerodynamics of Missile Fins," *Journal of Spacecraft and Rockets*, Vol. 20, No. 4, 1983, pp. 356–362. doi:10.2514/3.25606

[19] Smith, C. A., Nielsen, J. N., and Hemsch, M. J., "Prediction of Aerodynamic Characteristics of Cruciform Missiles to High Angles of Attack," AIAA Paper 79-0024, Aug. 1979.

[20] Uselton, B. L., and Jenke, L. M., "Experimental Missile Pitch- and Roll-Damping Characteristics at Large Angles of Attack," *Journal of Spacecraft and Rockets*, Vol. 14, No. 4, 1977, pp. 241–247. doi:10.2514/3.57188

[21] Cohen, C. J., Clare, T. A., and Stevens, F. L.," Analysis of the Nonlinear Rolling Motion of Finned Missiles," *AIAA Journal*, Vol. 12, No. 3, 1974, pp. 303–309. doi:10.2514/3.49225

[22] Pepitone, T. R., and Jacobson, I. D., "Resonant Behavior of a Symmetric Missile Having Roll Orientation-Dependent Aerodynamics," *Journal of Guidance and Control*, Vol. 1, No. 5, 1978, pp. 335–339. doi:10.2514/3.55789

[23] Reece, E. W., "Results of a Wind Tunnel Test to Determine the Effect of Roll Position on the Longitudinal Static Stability of the Tomahawk Rocket Configuration at Mach 7.3," Sandia Lab., SC-TM-66-495, Albuquerque, NM, Oct. 1966.

[24] Regan, F. J., Shermerhorn, V. L., Falusi, M. E., "Roll-Induced Force and Moment Measurements of the M823 Research Store," U.S. Naval Ordnance Lab TR 68-195, White Oak, MD, Nov. 1968.

[25] Bolz, R. E., "Dynamic Stability of a Missile in Rolling Flight," *Journal of the Aeronautical Sciences*, Vol. 19, No. 6, 1952, pp. 395–403.

[26] Benton, E. R., "Supersonic Magnus Effects on a Finned Missile," *AIAA Journal*, Vol. 2, No. 1, 1964, pp. 153–155. doi:10.2514/3.2252